Arf5-mediated regulation of mTORC1 at the plasma membrane

Christian Makhoul[a], Fiona J. Houghton[a], Elizabeth Hinde[a,b], and Paul A. Gleeson[a,*]
[a]Department of Biochemistry and Pharmacology and Bio21 Molecular Science and Biotechnology Institute and [b]School of Physics, The University of Melbourne, Melbourne, Victoria 3010, Australia

ABSTRACT **The mechanistic target of rapamycin (mTOR) kinase regulates a major signaling pathway in eukaryotic cells. In addition to regulation of mTORC1 at lysosomes, mTORC1 is also localized at other locations. However, little is known about the recruitment and activation of mTORC1 at nonlysosomal sites. To identify regulators of mTORC1 recruitment to nonlysosomal compartments, novel interacting partners with the mTORC1 subunit, Raptor, were identified using immunoprecipitation and mass spectrometry. We show that one of the interacting partners, Arf5, is a novel regulator of mTORC1 signaling at plasma membrane ruffles. Arf5-GFP localizes with endogenous mTOR at PI3,4P2-enriched membrane ruffles together with the GTPase required for mTORC1 activation, Rheb. Knockdown of Arf5 reduced the recruitment of mTOR to membrane ruffles. The activation of mTORC1 at membrane ruffles was directly demonstrated using a plasma membrane–targeted mTORC1 biosensor, and Arf5 was shown to enhance the phosphorylation of the mTORC1 biosensor substrate. In addition, endogenous Arf5 was shown to be required for rapid activation of mTORC1-mediated S6 phosphorylation following nutrient starvation and refeeding. Our findings reveal a novel Arf5-dependent pathway for recruitment and activation of mTORC1 at plasma membrane ruffles, a process relevant for spatial and temporal regulation of mTORC1 by receptor and nutrient stimuli.**

Monitoring Editor
JoAnn Trejo
University of California, San Diego

Received: Aug 1, 2022
Revised: Jan 18, 2023
Accepted: Jan 27, 2023

INTRODUCTION

A major intracellular signaling pathway of all eukaryotes is the mechanistic (or mammalian) target of rapamycin (mTOR) pathway. mTOR exists in two distinct kinase complexes, mTORC1 and mTORC2. mTORC1 controls growth, proliferation, and metabolism, whereas mTORC2 regulates cytoskeletal dynamics (Wullschleger *et al.*, 2006; Betz and Hall, 2013). mTORC1 is a Ser/Thr kinase that senses the nutritional and energy status of a cell and responds to growth factor signaling and amino acid availability. Under nutrient-rich conditions, mTORC1 triggers downstream responses via phosphorylation of a set of substrates, which includes promoting ribosome biogenesis, protein translation, nutrient import, and, in addition, inhibition of autophagy and stress responsive transcription (Sancak *et al.*, 2010).

The activation of mTORC1 is regulated by GTPases on the cytosolic surface of intracellular organelles. Most of the studies on the regulation of the mTORC1 signaling pathway have focused on the lysosomal membrane as a central hub for the recruitment and activation of mTORC1 (Betz and Hall, 2013). However, emerging studies are revealing that in addition to the lysosomes, mTORC1 can be spatially regulated at a number of cellular compartments including the plasma membrane, endoplasmic reticulum (ER), Golgi apparatus, and nucleus (Chao and Avruch, 2019; Makhoul and Gleeson, 2021). mTORC1 activation is facilitated through a direct interaction with membrane-associated Rheb GTPase, which drives a conformational change that promotes its kinase activity (Yang *et al.*, 2017). The role of Rheb in the activation of mTORC1 at the lysosomes is well defined (Lim and Zoncu, 2016; Angarola and Ferguson, 2020). Rheb has also been localized to a number of other cellular compartments, including the ER, Golgi, and peroxisomes (Buerger *et al.*, 2006; Yadav *et al.*, 2013; Zhang *et al.*, 2013; Gosavi *et al.*, 2018; Hao *et al.*, 2018;

This article was published online ahead of print in MBoC in Press (http://www.molbiolcell.org/cgi/doi/10.1091/mbc.E22-07-0302) on February 3, 2023.
Conflict of interest: The authors declare no conflict of interest.
*Address correspondence to: Paul Gleeson (pgleeson@unimelb.edu.au).
Abbreviations used: CDR, circular dorsal ruffles; FRET, Förster resonance energy transfer; mTOR, mechanistic target of rapamycin; TAPP1, tandem PH-domain–containing protein 1.

Angarola and Ferguson, 2019), suggesting that mTORC1 can be spatially regulated by distinct or possibly overlapping mechanisms at various sites within the cell. Spatial regulation is emerging as a theme for other signaling pathways, such as Toll-like receptor (TLR) 4 activation (Kagan *et al.*, 2008) where the cell surface and endosomes mediate different downstream outputs from the same receptor. Notably, there is growing evidence for a role of the secretory pathway in the regulation of mTORC1 signaling, in particular the Golgi apparatus (Liu and Zheng, 2007; Thomas *et al.*, 2014; Fan *et al.*, 2016; Gosavi *et al.*, 2018; Makhoul and Gleeson, 2021), and recently focal adhesions at the plasma membrane have also been suggested to act as mTORC1 signaling hubs (Rabanal-Ruiz *et al.*, 2021).

mTORC1 is a central regulator of cell growth and proliferation, and mTORC1 dysfunction contributes to various diseases such as cancer, neurodegeneration, and cardiovascular diseases (Perluigi *et al.*, 2015; Kim *et al.*, 2017; de la Cruz Lopez *et al.*, 2019). Defining the molecular components that regulate the recruitment and activation of mTORC1 to various intracellular compartments is essential to understanding the regulation of this key signaling pathway. However, there is a paucity of information on the factors responsible for recruitment and activation of mTORC1 to nonlysosomal locations. mTORC1 consists of five components, Raptor, PRAS40, Deptor, mLST8, and mTOR (Chao and Avruch, 2019). The recruitment of the mTORC1 complex from the cytosol to lysosome membranes is mediated by the interaction of Raptor with Rag GTPases on the cytosolic side of lysosomal membranes (Sancak *et al.*, 2010). To detect additional binding partners with Raptor that may regulate recruitment to nonlysosomal membranes, here we utilized myc-Raptor as the bait protein for immunoprecipitation and proteomic analysis of potential binding partners. From this analysis we have identified the GTPase Arf5 as a novel interactor of Raptor. Arf5 has been reported to localize to a number of subcellular compartments including the Golgi and the plasma membrane (PM) (Hasegawa *et al.*, 2012; Egerer *et al.*, 2015). Here, we show that Arf5 regulates mTORC1 recruitment to the cell periphery on membrane ruffles and mTORC1 signals at membrane ruffles, as demonstrated by the use of a plasma membrane–localized Förster resonance energy transfer (FRET) mTORC1 biosensor (Zhou *et al.*, 2015). In addition, Arf5 was shown to be required for rapid activation of mTORC1 following nutrient stimulation. Our findings highlight the contribution of the plasma membrane in mTORC1 signaling.

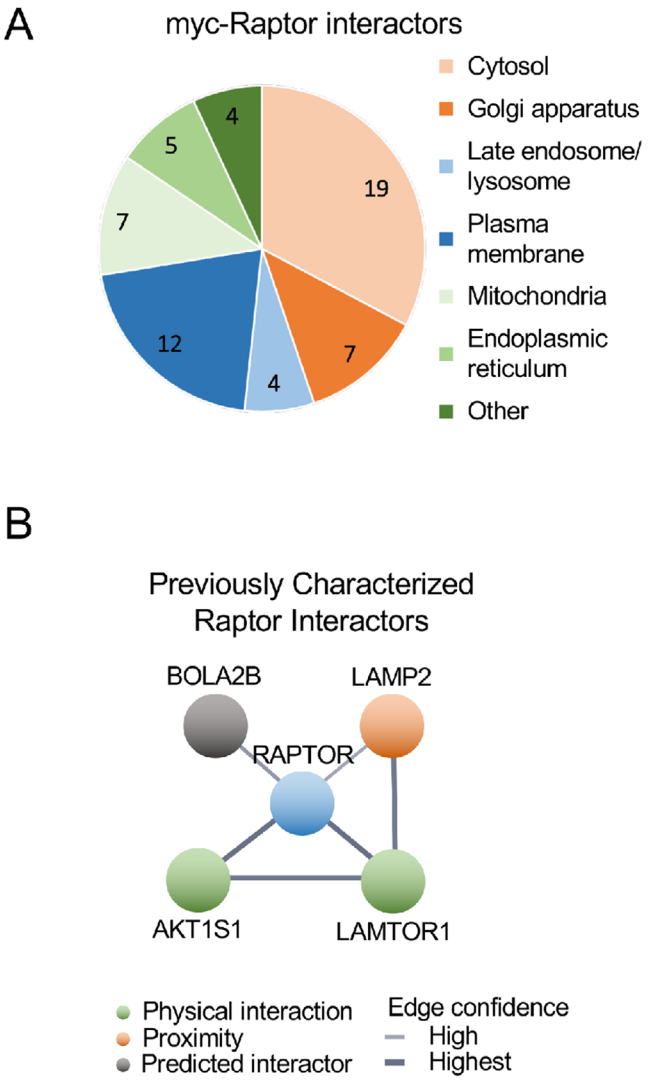

FIGURE 1: Identification of candidate membrane-associated interacting partners of myc-Raptor. (A) Summary of intracellular locations of myc-Raptor candidate interacting partners identified by immunoprecipitation and MS analysis. (B) Network of previously characterized Raptor-interacting partners that were identified using affinity chromatography.

RESULTS

Identification of potential mTORC1-interacting proteins using myc-Raptor as bait

Raptor is an integral subunit of mTORC1 and has been reported to guide the subcellular localization of this complex by interacting with Rag GTPases at the surface of lysosomes (Sancak *et al.*, 2008, 2010). We hypothesized that Raptor could also target mTORC1 to nonlysosomal compartments through site-specific interactions with different binding partners. To identify novel mTORC1-interacting proteins that regulate its recruitment to nonlysosomal compartments, we utilized myc-Raptor as the bait protein to coimmunoprecipitate candidate interactive proteins, which were identified by mass spectrometry (IP-MS). As a control to differentiate nonspecific proteins in the IP, myc-Rab6A(Q72L) was used. Myc-tagged proteins were efficiently expressed in HeLa cells and efficiently recovered by affinity chromatography using an antibody against the myc epitope (Supplemental Figure S1). Three independent IP experiments were performed and immunoprecipitates analyzed by MS. In total 44 proteins were identified as unique proteins from immunoprecipitates of myc-Raptor transfected cells, but not the myc-Rab6A(Q72L) transfected cells, in at least two of the three independent experiments (Supplemental Appendix Table 1). A STRING analysis of the myc-Raptor binding proteins revealed previously characterized Raptor interactors, namely, AKT1S1 (PRAS40), a regulatory subunit of mTORC1 that inhibits direct binding of substrates to the kinase complex (Wang *et al.*, 2007), and LAMTOR1, which is a subunit of the lysosomal Ragulator complex that plays an important role in amino acid–driven activation of mTORC1 (Figure 1B) (Sancak *et al.*, 2010; Bar-Peled *et al.*, 2012). In addition, LAMP2 and BOLA2B were also identified in the myc-Raptor pull down, and these components were also previously proposed to be interactors of Raptor (Go *et al.*, 2021). The identification of these known mTORC1 interactive proteins in the IP validated the methodology. The myc-Raptor candidate interactors were filtered to identify membrane-associated proteins by excluding proteins that were exclusively localized to the nucleus or cytosol. This yielded 31 unique proteins that were associated with a range of different intracellular membranes or membrane-bound organelles as illustrated by the pie charts in Figure 1A.

Most of the candidate interacting proteins identified in the IP have been reported to localize to more than one cellular compartment; hence the apparent discrepancies between the number of identified candidates and the total number of proteins that are represented in the pie chart.

The candidate interactors that particularly drew our attention were three small GTPases that were coimmunoprecipitated with myc-Raptor, namely ADP-ribosylation factor 5 (Arf5) and Ras-related proteins Rab15 and Rab35, as small G proteins contribute to the regulation of the mTORC1 signaling pathway on lysosomes, namely RagA/C and RagB/D, and it is likely that other small G proteins may regulate site-specific recruitment of mTORC1. Of the three small G proteins detected, Arf5 was identified as significant in all three independent experiments (Supplemental Appendix Table 1) and is the most well characterized of the three small G proteins. Arf5 has been reported to be localized to a number of different compartments, including the plasma membrane (Hasegawa *et al.*, 2012), Golgi (Chun *et al.*, 2008; Egerer *et al.*, 2015), and the ER-to-Golgi intermediate compartment (Chun *et al.*, 2008). We therefore investigated the potential role of Arf5 in membrane recruitment and activation of mTORC1.

Arf5 regulates mTORC1 recruitment to the plasma membrane

To assess the intracellular distribution of Arf5, HeLa cells were transiently transfected with wild-type (WT) Arf5-GFP and the location at the PM and Golgi assessed. As a control, cells were transfected with another GFP-tagged small G protein, namely WT Arf1-GFP, a well-characterized Golgi-resident Arf protein tagged with GFP (Donaldson *et al.*, 2005). Arf5-GFP colocalized with the *trans*-Golgi network (TGN) marker, golgin-245, and was also localized at the cell periphery on membrane ruffles (Supplemental Figure S2A). The detection of Arf5 at the plasma membrane is consistent with previous reports (Moravec *et al.*, 2012). In contrast, the localization of Arf1-GFP was predominantly restricted to the Golgi (Supplemental Figure S2A). To determine whether exogenous Arf5 expression influences the recruitment of mTOR to the PM or Golgi, Arf5-GFP transfected HeLa cells were costained for golgin-245 and mTOR. The Arf5-GFP signal colocalized with mTOR at the cell periphery on membrane ruffles (Figure 2A), indicating a spatial association of Arf5-GFP with mTOR at membrane ruffles.

To further investigate the behavior of Arf5 at membrane ruffles and to eliminate the possibility of indirect effects of the GFP fusion, an epitope-tagged version of Arf5 was used (WT Arf5-HA) and cotransfected with a fluorescent marker for membrane ruffles, namely a mCherry-tagged chimera of the TAPP1 (tandem PH-domain–containing protein 1) C-terminal PH domain (mCherry-TAPP1-C-PH). The C-terminal pleckstrin homology (PH) domain of TAPP1 acts as a marker for membrane ruffles by binding to phosphoinositol 3,4-bisphophate (PI3,4P), which is enriched at this site (Thomas *et al.*, 2001; Lenoir *et al.*, 2015). As for WT Arf5-GFP, HA-tagged WT Arf5 was also localized to the plasma membrane, where it colocalized with mCherry-TAPP1-C-PH (Figure 2B). In addition, HeLa cells were costained for mTOR; the mTOR signal colocalized with Arf5-HA (Figure 2B). To validate the specificity of the mTOR signal that is being detected at membrane ruffles, mTOR was depleted in Arf5-GFP transfected HeLa cells by RNA interference, and the cells were subsequently stained with mTOR antibodies. The depletion of mTOR abolished the staining with mTOR antibodies and, in particular, there was an absence of antibody staining on Arf5-GFP–positive membrane ruffles (Figure 2C), which confirmed the specificity of the mTOR signal. The efficiency of mTOR knockdown was analyzed by immunoblotting of cell extracts; mTOR small interference RNA (siRNA)-treated cells showed an ~80% reduction in the total levels of mTOR compared with the control (Figure 2D).

Because mTOR colocalized with Arf5 in HeLa cells, the next step was to validate whether Arf5 interacts with mTORC1 through the Raptor subunit. To characterize the interaction between Arf5 and myc-Raptor, the WT and GTP-bound (Q71L) and GDP-bound (T31N) variants of HA-tagged Arf5 were cotransfected with myc-Raptor in HeLa cells. As a control to assess nonspecific interactions of HA-tagged proteins, we used Arl5-BirA*-HA. In cell lysates, antibody to HA detected the HA-Arf5 variants at ~20 kDa and Arl5b-BirA*-HA just below the 50 kDa marker, sizes consistent with their expected molecular masses (Figure 2E). Cell extracts were immunoprecipitated with anti-myc antibody and the immunoprecipitates analyzed by immunoblotting. myc-Raptor was precipitated in all samples and was detected at ~150 kDa, consistent with its expected size (Figure 2E). Blotting the IP samples with HA antibody revealed that the WT and GDP-bound (T31N) Arf5 variant, but not the GTP-bound (Q71L) form, were coprecipitated with myc-Raptor (Figure 2E). The heavy and light chains of the mouse anti-myc antibody that was used to immunoprecipitate myc-Raptor were also detected in the blot (*; Figure 2E) but did not mask the signal of the HA constructs. Arl5-BirA*-HA was not detected in the IP sample. Taken together, these data indicate that the interactions of HA-tagged Arf5 proteins with myc-Raptor were specific. Combined with the MS and immunofluorescence data, the coimmunoprecipitation results provided further evidence that Arf5 interacts, either directly or indirectly, with mTORC1 through Raptor. The Arf5-T31N variant also strongly localized to membrane ruffles (Supplemental Figure S2B). The plasma membrane association of Arf5-T31N-HA was an unexpected finding as GDP-bound mutants are not typically targeted to membranes, although some studies have documented that Arf5 can be peripherally targeted to membranes in the GDP-bound form (Chun *et al.*, 2008; Sadakata *et al.*, 2010).

To investigate the potential relevance of Arf5 and mTORC1 at the cell surface, two issues were next addressed. First, immunofluorescence staining with mTOR antibodies does not differentiate between mTORC1 and mTORC2; therefore it was important to validate that mTORC1 is localized to membrane ruffles and, second, to determine whether Arf5 had a role in the recruitment of mTOR to membrane ruffles. To address these questions quantitatively, HeLa cells were treated with either 1) control, 2) mTOR, 3) Raptor, or 4) Arf5 siRNA and transfected with mCherry-TAPP1-C-PH to identify membrane ruffles (Figure 3A). Cells were then fixed and stained with a mTOR antibody. The mCherry signal was used to generate a mask of the membrane ruffles using Fiji image analysis software (Figure 3A), and the mean fluorescence intensity (MFI) of mTOR was quantified within this masked region. Immunoblotting showed selective reduction in the levels of mTOR, Raptor, and Arf5 after treatment with specific siRNA (Figure 3B). Analysis of 12 cells from two independent experiments showed an ~76% reduction in mTOR fluorescence intensity after treatment with mTOR siRNA, which validated the specificity of mTOR staining at membrane ruffles in this experiment and provided a positive control for comparison (Figure 3C). Depletion of Raptor led to an ~47% reduction in the mean fluorescence intensity of mTOR within the masked region (Figure 3C), and as Raptor is specifically associated with mTORC1 but not mTORC2 (Hara *et al.*, 2002; Sarbassov *et al.*, 2004), this finding demonstrated that mTORC1 is present at these membrane ruffles. Finally, depletion of Arf5 showed a significant reduction (~25%) in the mean fluorescence intensity of mTOR at membrane ruffles (Figure 3C). Collectively, these data suggest that Arf5 contributes to the recruitment of mTORC1 at PM ruffles.

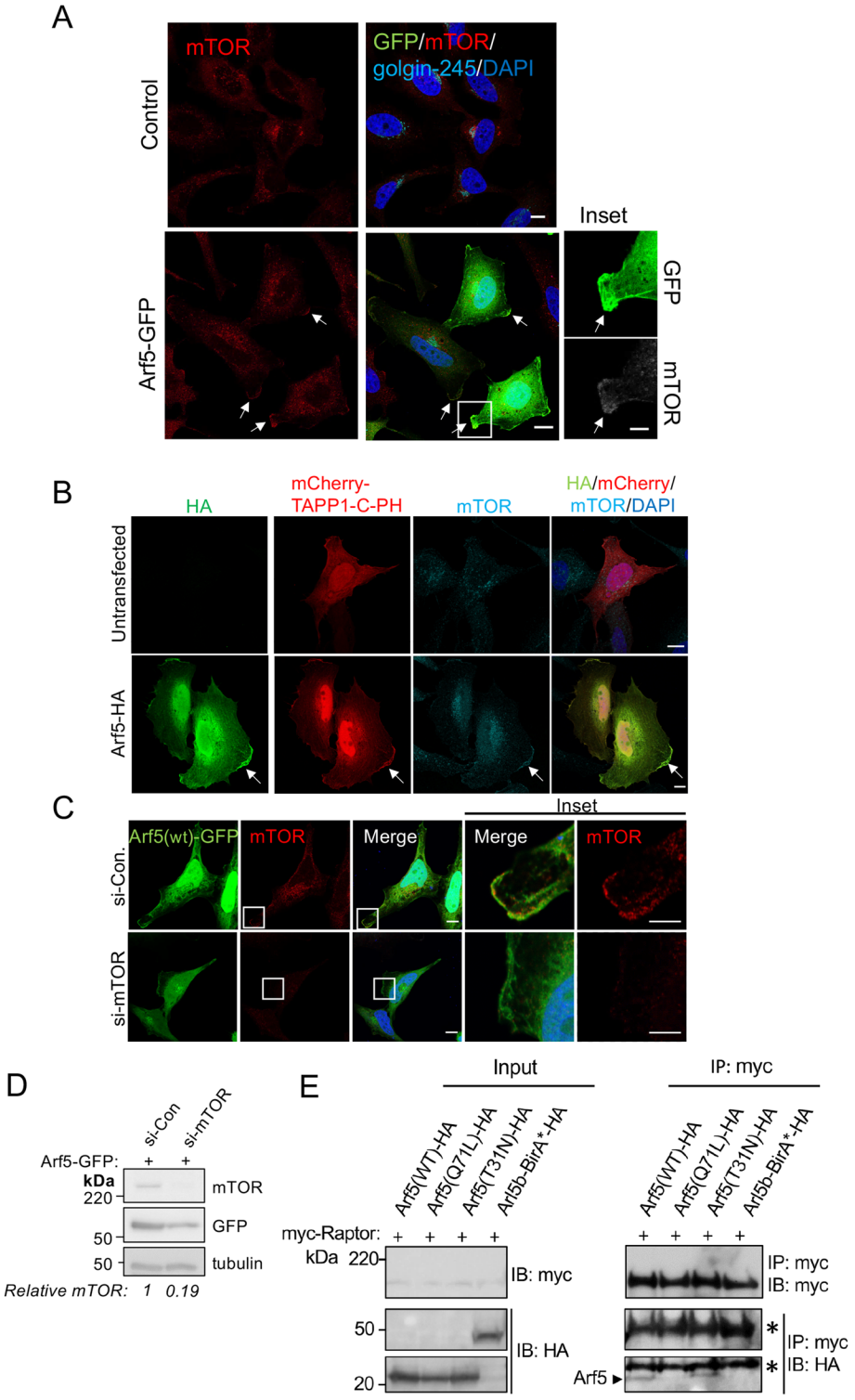

FIGURE 2: mTOR colocalized with HA-tagged Arf5 at peripheral ruffles. (A) HeLa cell monolayers were either left untransfected or transfected with Arf5-GFP for 24 h. Cells were fixed, permeabilized, and stained with human anti–golgin-245 (pseudocolored cyan) or rabbit anti-mTOR (red). Nuclei were stained with DAPI. Images represent single optical sections. Boxed regions have been digitally magnified (inset). Scale bar, 10 μm, 5 μm for the inset. Of 49 Arf5-GFP–expressing cells imaged from three independent experiments, 28 cells (57.1%) showed Arf5-GFP localization at the cell periphery on membrane ruffles. All 28 cells showed colocation between Arf5-GFP with endogenous mTOR. (B) HeLa cell monolayers were cotransfected with mCherry-TAPP1-C-PH and Arf5(WT)-HA for 24 h. Control cells were transfected with only mCherry-TAPP1-C-PH. Cells were fixed, permeabilized, and stained with mouse anti-HA (green) and rabbit anti-mTOR (cyan). Images represent compressed z-stacks. Scale bar, 10 μm. Of 33 cells expressing Arf5-HA imaged from two independent experiments, 21 (64%) of Arf5-HA–expressing cells showed a peripheral signal for Arf5 on membrane ruffles, all of which colocated with endogenous mTOR. (C, D) HeLa cell monolayers were transfected with either control or mTOR siRNA for 48 h and then transfected with Arf5-WT-GFP for 24 h. (C) Cells were fixed and stained with rabbit anti-mTOR (red), and the nucleus was stained with DAPI (blue). Images represent compressed z-stacks. Boxed regions have been digitally magnified (inset). Scale bar, 10 μm, 5 μm in the inset. (D) Cell extracts were harvested and analyzed by immunoblotting. Using the molecular weight marker as a guide, the PVDF membrane was cut and probed with rabbit anti-mTOR and mouse anti-GFP, and the images were developed using a chemiluminescence system. The membrane that was probed with mouse anti-GFP was then stripped and reprobed with mouse anti–α-tubulin, which was used as a loading control to quantify the relative levels of mTOR. (E) HeLa cell monolayers were cotransfected with myc-Raptor and one of the following: Arf5(WT)-HA, Arf5(Q71L)-HA, Arf5-(T31N)-HA, or Arl5b-BriA*-HA. myc-Raptor and its interacting partners were immunoprecipitated with myc antibodies. Using the molecular weight marker as a guide, the PVDF membrane was cut and the total (input) and immunoprecipitated (IP) samples were analyzed by immunoblotting with a rabbit anti-HA and a mouse anti-myc antibody using a chemiluminescence detection system. The IP blot (right panel) was exposed for twice as long to increase the detection sensitivity. The heavy and light chains of the myc antibody were detected in the immunoprecipitated samples at 50 and 25 kDa (indicated by *), and Arf5 was detected at 20 kDa (indicated by ▶). Shown is a representative example of three independent experiments.

To determine whether Arf5 depletion affected the recruitment of mTORC1 to the lysosomes, HeLa cells were treated with either control or Arf5 siRNA, fixed, and costained with antibodies against mTOR and CD63. Analysis by confocal microscopy showed prominent colocalization of mTOR with the late endosome/lysosome marker CD63 in both control siRNA–treated cells and Arf5 siRNA–treated cells (Figure 3D). Moreover, to determine the proximity of CD63-positive lysosomes to membrane ruffles, a line scan analysis demonstrated good overlap of mTOR and CD63 in punctate intracellular structures, whereas no overlap of CD63 was detected on the mTOR-positive membrane ruffles (Supplemental Figure S3),

demonstrating spatial separation between the mTOR detected on membrane ruffles and CD63-positive lysosomes. These findings indicated that Arf5 is important for mTOR localization at membrane ruffles but does not appear to contribute to the recruitment of mTORC1 to lysosomes.

mTORC1 is colocated with EGF receptor and Rheb at the plasma membrane

External stimuli, such as growth factor receptor signaling, is a major upstream regulator of mTORC1 activation. However, information on potential mTORC1 activation at the plasma membrane is very limited, and therefore we explored the relationship between growth factor receptor activation and mTORC1 at the plasma membrane. First, we examined the spatial relationship of mTOR and epidermal growth factor receptor (EGFR) in HeLa cells that were either serum starved overnight or serum starved and then supplemented with 25 ng/ml EGF for 3 min (Figure 4A). Following a 16-h period of serum starvation, endogenous mTOR staining was heterogeneous throughout the cytoplasm with cytosolic and intracellular membrane–associated staining and with very little detected at the cell periphery, as defined by phalloidin staining of F-actin to detect cortical actin (Figure 4A). After a 3-min stimulation with EGF, mTOR signal was detected at the cell periphery and was juxtaposed with EGFR staining (Figure 4A). The observation that mTOR was in close proximity to EGFR at the PM has potential relevance to the transduction of the EGFR signaling cascade.

Membrane ruffling is a response to extracellular stimuli that promotes mTOR activation (Yoshida *et al.*, 2015). We selected a specialized cell line with more extensive ruffling than HeLa cells to investigate the distribution of mTOR at the plasma membrane. The RAW264.7 cell line is a mouse macrophage cell line that exhibits extensive constitutive ruffling, typical of primary macrophages (Lin *et al.*, 2020). RAW264.7 cells were cultured in complete growth medium and stained with a mTOR antibody and a phalloidin-TRITC conjugate, an F-actin probe to mark membrane ruffles. Superresolution imaging using an Airyscan detector coupled with Huygens deconvolution showed extensive phalloidin-positive staining of membrane ruffles in RAW264.7 cells, and furthermore, there was extensive colocalization between mTOR and phalloidin-TRITC at these membrane ruffles (Figure 4B). Activation of mTORC1 requires the upstream regulator, Rheb, a small G protein that is essential for the activation of mTORC1 kinase activity (Long *et al.*, 2005). RAW264.7 cells were also stained with antibodies against Rheb. In RAW264.7 cells, Rheb and mTOR are both located at sites of phalloidin-positive membrane ruffles (Figure 4B); the superresolution images using the above protocol have a lateral resolution of ~100 nm (Fourriere *et al.*, 2022) and demonstrated the proximity of Rheb and mTOR within these membrane ruffles (Figure 4B, inset). This finding indicates that mTOR is located at membrane ruffles together with Rheb, suggesting that mTORC1 could be activated at the PM.

Detection of mTORC1 activation at the PM with a biosensor

The above findings indicated that mTORC1 activity may be regulated at the PM. Next, we sought to directly examine the activation of mTORC1 at membrane ruffles. To this end we used the plasma membrane–targeted mTORC1 biosensor, PM-TORCAR, that was previously developed by Zhou *et al.* (2015). TORCAR consists of the mTORC1 substrate, 4E-BP1, flanked by the Cerulean and YPet FRET pair on its amino terminus and carboxyl terminus, respectively (Figure 5A). PM-TORCAR has the Lyn kinase PM-targeting motif on the N-terminus of the TORCAR biosensor, which is reported to efficiently direct PM-TORCAR to the cell surface of NIH3T3 cells. Phosphorylation of two specific sites on 4E-BP1, namely threonine 37 and 46 (T37/46), by mTORC1 drives a conformational change in 4E-BP1 that separates the Cerulean-YPet pair and leads to a reduction in FRET (Zhou *et al.*, 2015). Conversely, mTORC1 kinase inhibition prevents phosphorylation of the biosensor pseudosubstrate, which enhances the FRET efficiency.

We confirmed the location of PM-TORCAR in transfected HeLa cells. PM-TORCAR was detected by YFP fluorescence and, as observed with Z stacks of XY optical sections, was highly prominent at the PM boundary of the cell, especially enriched in mCherry-TAPP1-C-PH–positive structures. PM-TORCAR fluorescence was also associated with ruffle-like structures within the cell boundary, which probably reflects the dorsal surface of the cell, a conclusion confirmed by analysis of Y stacks of XZ optical sections (Figure 5B). The latter clearly shows the fluorescence restricted to the dorsal and lateral surfaces; in particular, the fluorescence on the dorsal surface is enriched in membrane ruffles. Hence these data demonstrate that the PM-TORCAR is restricted to the PM in transfected HeLa cells and is concentrated in membrane ruffles (Figure 5B).

To confirm that the biosensor was responsive to mTORC1 inhibition and activation, HeLa cells were transfected with PM-TORCAR and subjected to overnight serum starvation followed by 2 h of amino acid starvation (herein, double starvation). Following amino acid starvation, cells were nutrient replenished in complete growth media for 45 min and the cell extracts were harvested in a cell lysis buffer containing protease and phosphatase inhibitors. Immunoblotting analysis of the cell extracts was carried out to quantify the phosphorylated levels of the biosensor using a phospho-specific antibody targeted against the mTORC1 phosphorylation site on 4E-BP1 (T37/46). Phosphorylated PM-TORCAR has a molecular mass of ~75 kDa, which is distinguished from endogenous 4E-BP1 (15–20 kDa). Levels of phospho-T37/46 PM-TORCAR were normalized to the total levels of the biosensor using a polyclonal GFP antibody that recognizes Cerulean-YPet components of the biosensor. The analysis showed that double starvation reduced the phosphorylation levels of PM-TORCAR to 58% (Figure 5C). Phosphorylation of the surrogate biosensor substrate, 4E-BP1, is more resistant to starvation than endogenous mTORC1 substrates (unpublished data), and a reduction in PM-TORCAR phosphorylation of >50% after double starvation was difficult to obtain. Nutrient replenishment successfully recovered PM-TORCAR phosphorylation to 90% of the prestarved condition (Figure 5C). To validate that the recovery of phospho-PM-TORCAR was mTORC1 driven, the cells were also replenished with C-DMEM in the presence of mTOR/mTORC1 inhibitors, rapamycin, Torin-1, and wortmannin. Rapamycin, a macrolide reported to act as a specific inhibitor of mTORC1 (Brown *et al.*, 1994), showed no effect on the recovery of PM-TORCAR phosphorylation (Figure 5C). This result may be attributed to a previous finding that reported that 4E-BP1 is phosphorylated at T46 by rapamycin-insensitive activity of mTORC1 (Livingstone and Bidinosti, 2012). On the other hand, rapamycin treatment successfully inhibited the recovery of the phosphorylation of the mTORC1 endogenous substrate, ribosomal protein S6, using the same double starvation and replenishment protocol (Figure 5D). Thus, in the context of the biosensor 4E-BP1 substrate, rapamycin did not act as an effective inhibitor of mTORC1. Two other mTORC1 inhibitors were included, namely, the ATP-competitive mTOR inhibitor, Torin-1, and wortmannin, which inhibits phosphatidylinositol-3-kinase (PI3K), an upstream activator of mTORC1 (Wymann *et al.*, 1996; Walker *et al.*, 2000). Both inhibitors prevented the recovery of PM-TORCAR phosphorylation during nutrient replenishment (Figure 5C). Also, and as expected, Torin-1 and wortmannin inhibited the phosphorylation of S6

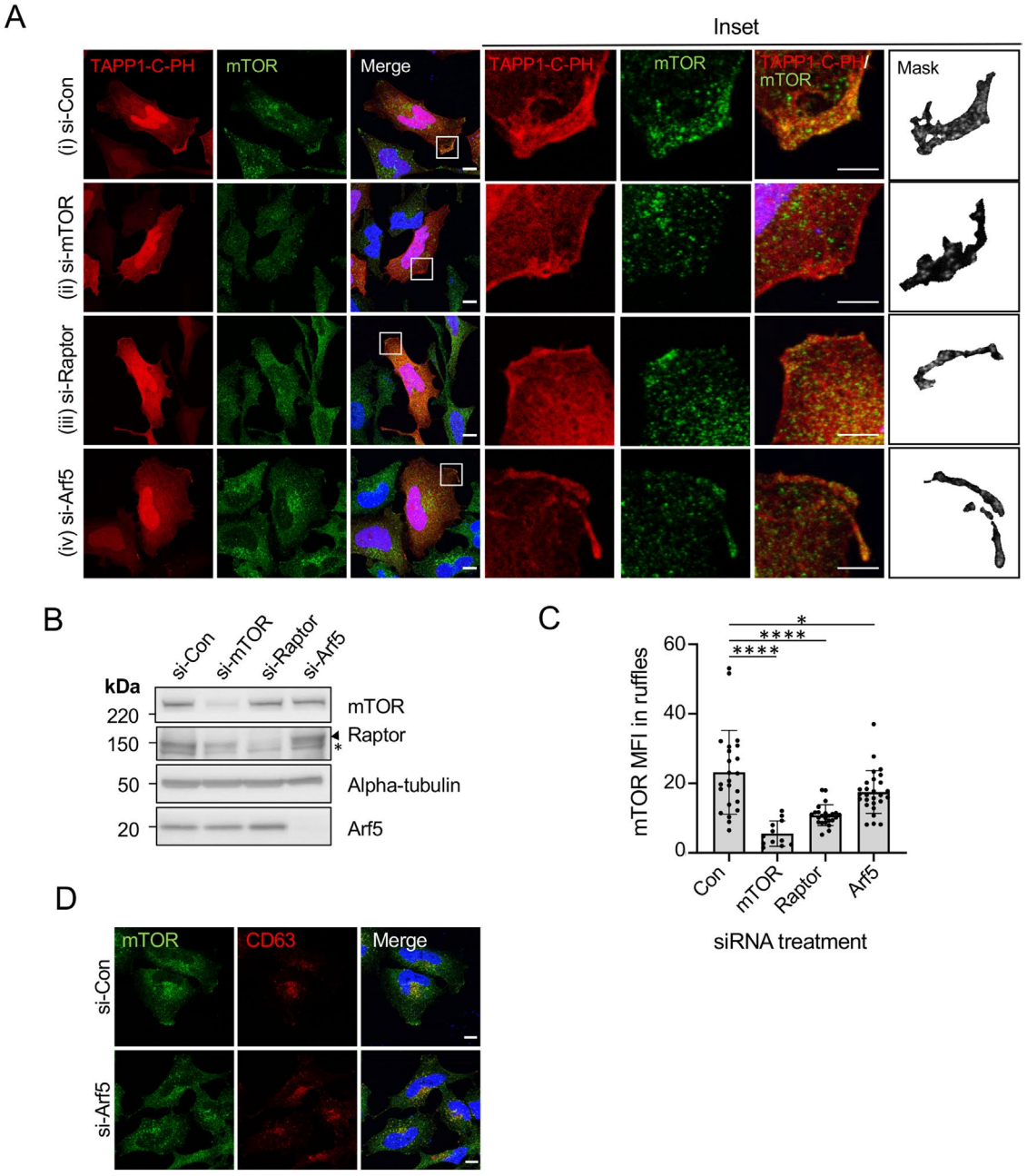

FIGURE 3: Arf5 promotes recruitment of mTORC1 to membrane ruffles. (A, C) HeLa cell monolayers were treated with siRNA as indicated and then transfected with mCherry-TAPP1-C-PH (red) for 24 h. (A) Cells were fixed and stained with rabbit anti-mTOR (green). The nucleus was visualized using DAPI (blue). Images represent compressed z-stacks. Boxed regions were digitally magnified (inset). Scale bar, 10 μm, 5 μm for the inset. Using the mCherry-TAPP1-C-PH signal, Fiji image analysis software was used to generate a mask of the peripheral ruffles and quantify the mean fluorescence intensity (MFI) of mTOR within this area in C. (B) HeLa cell extracts were analyzed by immunoblotting. Using the molecular weight marker as a guide, the PVDF membrane was cut and probed with rabbit anti-mTOR, rabbit anti-Raptor, mouse anti-Arf5, or mouse anti–α-tubulin as indicated. Images were developed using a chemiluminescence system to confirm the depletion of the desired targets. * indicates a nonspecific band detected with the Raptor antibody, and ▶ indicates the band that corresponds to Raptor. The blot is representative of two independent experiments. (C) mTOR MFI was quantified from the two independent experiments and is represented as a histogram with individual values. n (control) = 23, n (si-mTOR) = 12, n (si-Raptor) = 24, n (siArf5) = 27. *$p < 0.05$, ****$p < 0.0001$. Error bars represent SD. (D) HeLa cell monolayers were treated with control or Arf5 siRNA as indicated for 72 h. Cells were fixed and stained with rabbit anti-mTOR and mouse anti-CD63 (red), and the nucleus was visualized with DAPI (blue). Images represent compressed z-stacks. Scale bar, 10 μm.

following nutrient replenishment (Figure 5D). Collectively these data demonstrate that the PM-TORCAR biosensor was responsive to mTORC1 activation at the PM.

We examined the changes in PM-TORCAR phosphorylation in response to Arf5 overexpression. HeLa cells were either transfected with PM-TORCAR alone or cotransfected with Arf5-GFP, and cell

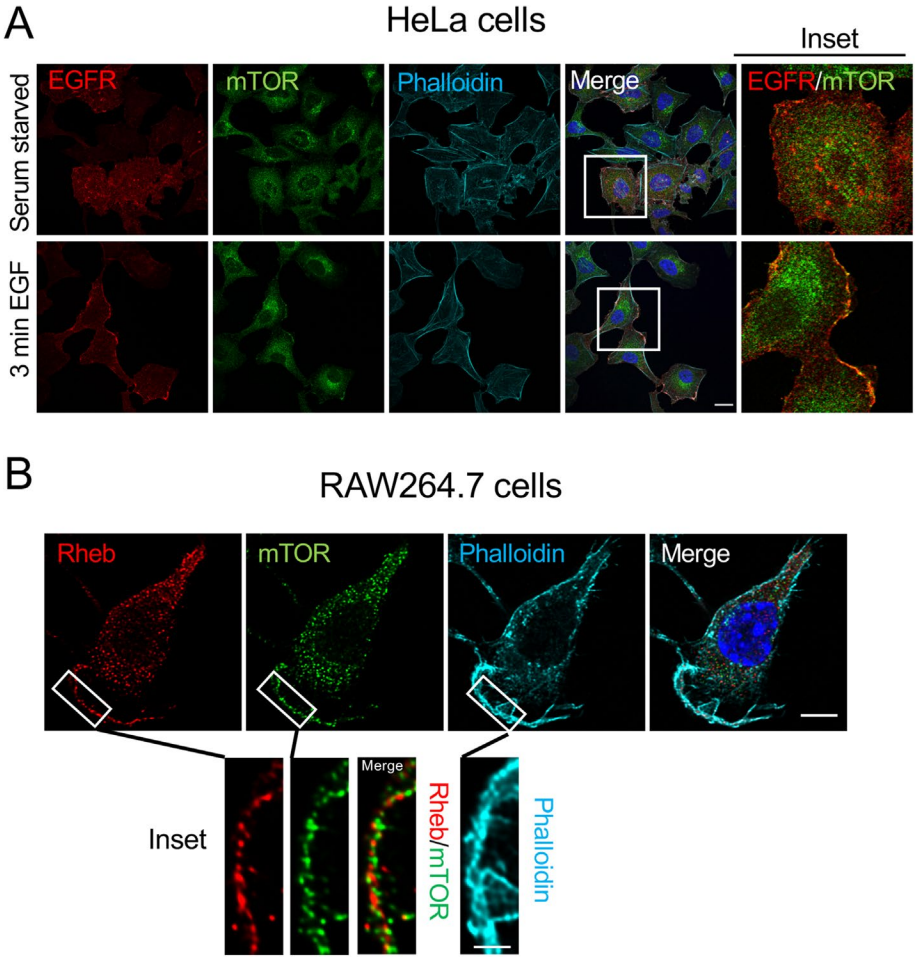

FIGURE 4: Localization of mTOR and Rheb to peripheral ruffles in HeLa cells and RAW264.7 macrophages. (A) mTOR is recruited to peripheral ruffles after EGF stimulation: HeLa cell monolayers were serum starved overnight and then stimulated with 25 ng/ml hEGF for 3 min. Cells were immediately fixed and stained with mouse anti-EGFR (red) and rabbit anti-mTOR (green). Actin was visualized using phalloidin-TRITC (cyan), and the nucleus was visualized using DAPI (blue). Images represent compressed z-stacks. Boxed regions were digitally magnified (inset) and show only the mTOR and EGFR staining pattern. Scale bar, 20 μm. Forty-seven EGF-stimulated cells were imaged across two independent experiments, and 64% showed colocation of mTOR with EGFR at the cell periphery. (B) Rheb is localized to peripheral ruffles in RAW264.7 cells: RAW264.7 cell monolayers were fixed and stained with mouse anti-Rheb (red) and rabbit anti-mTOR (green). Peripheral ruffles were visualized by staining actin filaments with phalloidin-TRITC (cyan). The nucleus was visualized with DAPI stain. Scale bar, 5 μm, inset 2 μm. Images represent a single optical section and were taken using Airyscan and then deconvoluted with Hyugens deconvolution software. From two independent staining experiments, all RAW264.7 cells with ruffles show similar staining patterns as shown.

extracts were analyzed by immunoblotting to quantify changes in PM-TORCAR phosphorylation (Figure 6A). Under steady state conditions, the immunoblotting analysis showed a 20% increase in PM-TORCAR phosphorylation in Arf5-GFP–expressing cells and double starvation led to a 50% reduction in PM-TORCAR phosphorylation relative to the prestarved conditions in both samples (Figure 6A). Nutrient replenishment (re-fed) led to a 20% higher level of PM-TORCAR phosphorylation in Arf5-GFP–expressing cells compared with the control cells (Figure 6). Nutrient replenishment was also performed in the presence of rapamycin, Torin-1, or wortmannin. In the presence of Torin-1 and wortmannin, PM-TORCAR phosphorylation was reduced in both control and Arf5-GFP–expressing cells (Figure 6A), indicating that the phosphorylation of the biosensor induced by Arf5-GFP expression was mTORC1 dependent. Rapamycin did not inhibit PM-TORCAR phosphorylation in control or Arf5-GFP transfected cells, consistent with the above finding. To quantify the impact of Arf5-GFP expression on the increase in PM-TORCAR phosphorylation, six independent replicates compared the changes in PM-TORCAR phosphorylation relative to the total expression level of the biosensor. Arf5-GFP coexpression with PM-TORCAR led to a statistically significant increase of 1.68-fold in the relative level of biosensor phosphorylation (Figure 6B).

The previous findings indicate that Arf5-GFP overexpression increased mTORC1 activity at the PM. To validate that the PM-TORCAR phosphorylation changes detected by immunoblotting were localized to the PM, we used fluorescence lifetime imaging microscopy (FLIM) to measure FRET changes in the PM-TORCAR. To perform this analysis, we also generated a donor-only control whereby the C-terminal YPet molecule was truncated from PM-TORCAR. This truncated biosensor is tagged only with Cerulean (hereon referred to as donor control) and represents a nonquenched donor in the FLIM-FRET imaging experiments. The donor control has a lifetime of ~3.0 ns (Figure 7A), which is similar to the reported lifetime of free Cerulean in the absence of FRET (Rizzo *et al.*, 2004). To investigate whether Arf5 expression affects the lifetime of the biosensor at the PM, HeLa cells were cotransfected with PM-TORCAR and either Arf5-mCherry or free mCherry as a control. Cells were then double starved and replenished with complete growth media for 45 min before imaging. Confocal images demonstrated the expression levels of PM-TORCAR and mCherry or Arf5-mCherry (Figure 7B). Changes in PM-TORCAR lifetime were then analyzed in these samples using the phasor approach to FLIM-FRET analysis (Hinde *et al.*, 2012). This involved transforming the lifetime of Cerulean within each pixel of each acquired FLIM image into a phasor and quantification of the extent to which the resulting phasor distribution is quenched due to FRET. Under steady state conditions, the PM-TORCAR biosensor gave rise to low and high FRET states with respect to the donor control (Figure 7A) that corresponded to the phosphorylated versus dephosphorylated state of mTOR. Phasor cursors defined to detect these two states enabled construction of FRET images that spatially map the phosphorylation state of mTORC1 (Figure 7B). The FRET images of PM-TORCAR showed a difference between the mCherry- and Arf5-mCherry transfected cells (Figure 7B). Whereas the PM biosensor was detected at the cell surface of mCherry-expressing cells in both high FRET (nonphosphorylated state; Figure 7B, red arrows) and low FRET (phosphorylated state), in Arf5-mCherry transfected cells most of the PM-TORCAR persisted in a low FRET state (phosphorylated)

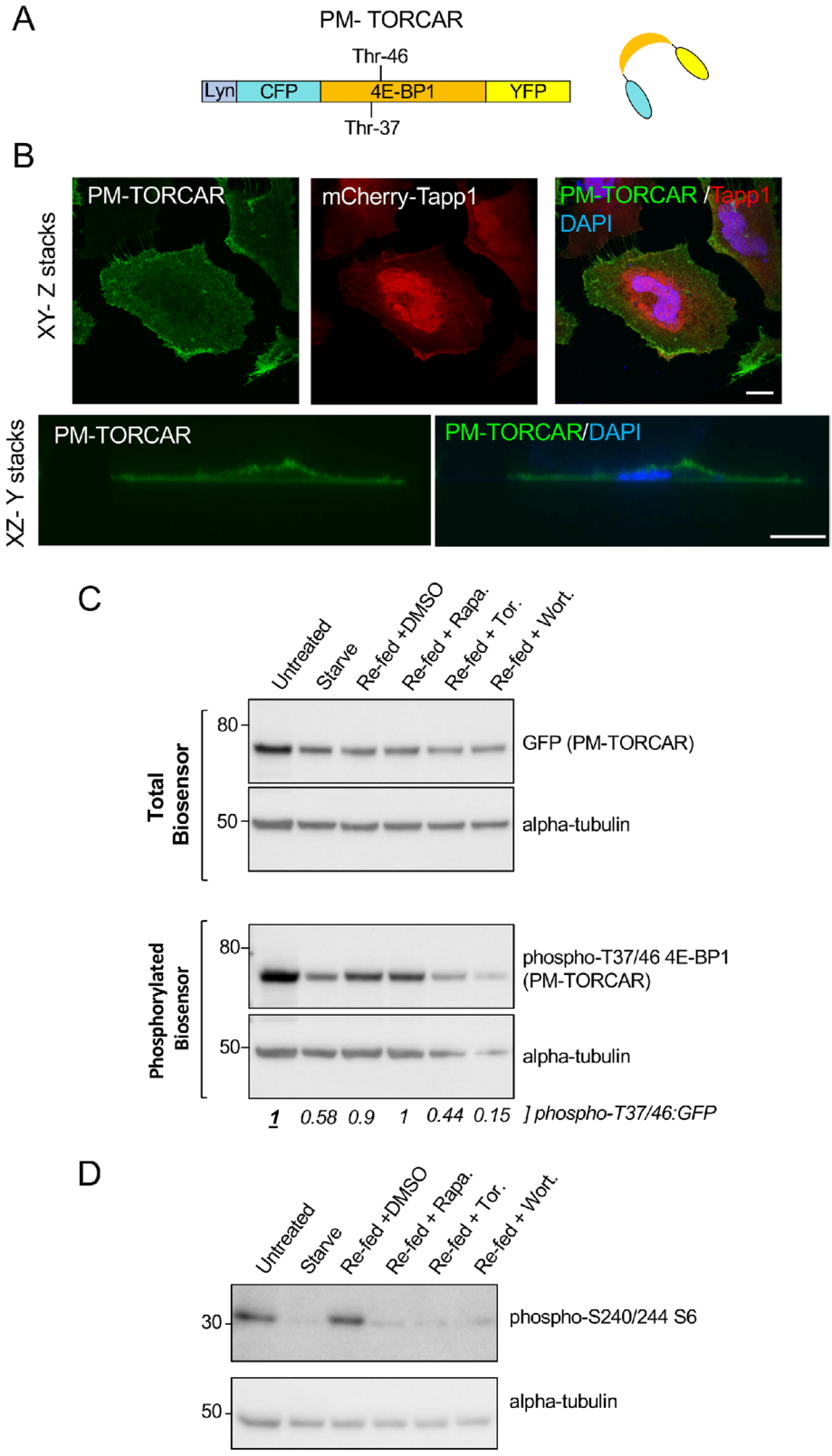

FIGURE 5: Phosphorylation of PM-TORCAR is modulated by nutrient starvation and refeeding. (A) Schematic of the PM-TORCAR construct consisting of the mTORC1 substrate, 4E-BP1, flanked by the CFP (Cerulean) and YFP (YPet) FRET pair on its amino terminus and carboxyl terminus, respectively, and the Lyn-targeting motif on the N-terminus (Lyn). Threonine 37 and 46 (Thr37/46) are phosphorylation sites. (B) Confocal images of HeLa cells transfected with PM-TORCAR (psudocolored green) and mCherry-TAPP1-C-PH (red) for 24 h. Nuclei were stained with DAPI. Shown are Z and Y stacks. Scale bar, 10 μm. (C) HeLa cell monolayers were transfected with PM-TORCAR for 24 h and then starved overnight in serum-free media. Cells were further starved for 2 h in amino acid–free media (EBSS) for 2 h before being refed with complete growth media (C-DMEM) for 45 min in the absence (DMSO) and presence of direct or indirect mTORC1 inhibitors (rapamycin, Torin-1, and wortmannin). Cell extracts were identically loaded onto separate protein gels and analyzed by immunoblotting. Using the molecular weight marker as a guide, the PVDF membranes were cut and probed with polyclonal rabbit anti-GFP (total biosensor), rabbit anti–phospho-T37/46 4E-BP1 (phosphorylated biosensor), and α-tubulin. Total and phosphorylated levels of the biosensor were normalized against α-tubulin to give the ratio of phosphorylated to total biosensor (phospho-T37/46:GFP). Changes in the phospho-T37/46:GFP ratio are relative to the untreated sample. (D) Samples from C were also run on a separate gel and analyzed by immunoblotting with rabbit anti–phospho-S240/244 S6 and mouse anti–α-tubulin. All images were developed using a chemiluminescence system. Shown is one of two independent experiments with similar data.

at membrane ruffles as indicated by the cyan arrows (Figure 7B). To quantify the differences between free mCherry and Arf5-mCherry transfected cells, the fractions of pixels in which the biosensor exhibited high FRET were compared between both samples (Figure 7C). The fraction of pixels in high FRET was significantly reduced by 23% in Arf5-mCherry–expressing cells compared with the mCherry control (Figure 7C) (mCherry control 0.63 ± 0.18; Arf5-mCherry 0.48 ± 0.21; mean ± SD, $n = 16$). This result indicates that, upon ectopic expression of Arf5-mCherry, the biosensor was more heavily phosphorylated due to increased mTORC1 activity at membrane ruffles and at the plasma membrane.

Arf5 regulates mTORC1 activity at the plasma membrane

The previous data show that Arf5 facilitates the recruitment of mTOR to the membrane ruffles, that mTORC1 can be activated on ruffles, and that PM-TORCAR can detect mTORC1 signaling selectively at the PM. To confirm that Arf5 is important in driving mTORC1-mediated phosphorylation of PM-TORCAR, HeLa cells were depleted of Arf5 and then transfected with PM-TORCAR. The phosphorylation of PM-TORCAR was then analyzed by immunoblotting under steady state or double-starved and nutrient-replenished conditions (Supplemental Figure S4). Starvation and nutrient replenishment in Arf5-depleted cells failed to recover PM-TORCAR phosphorylation during this

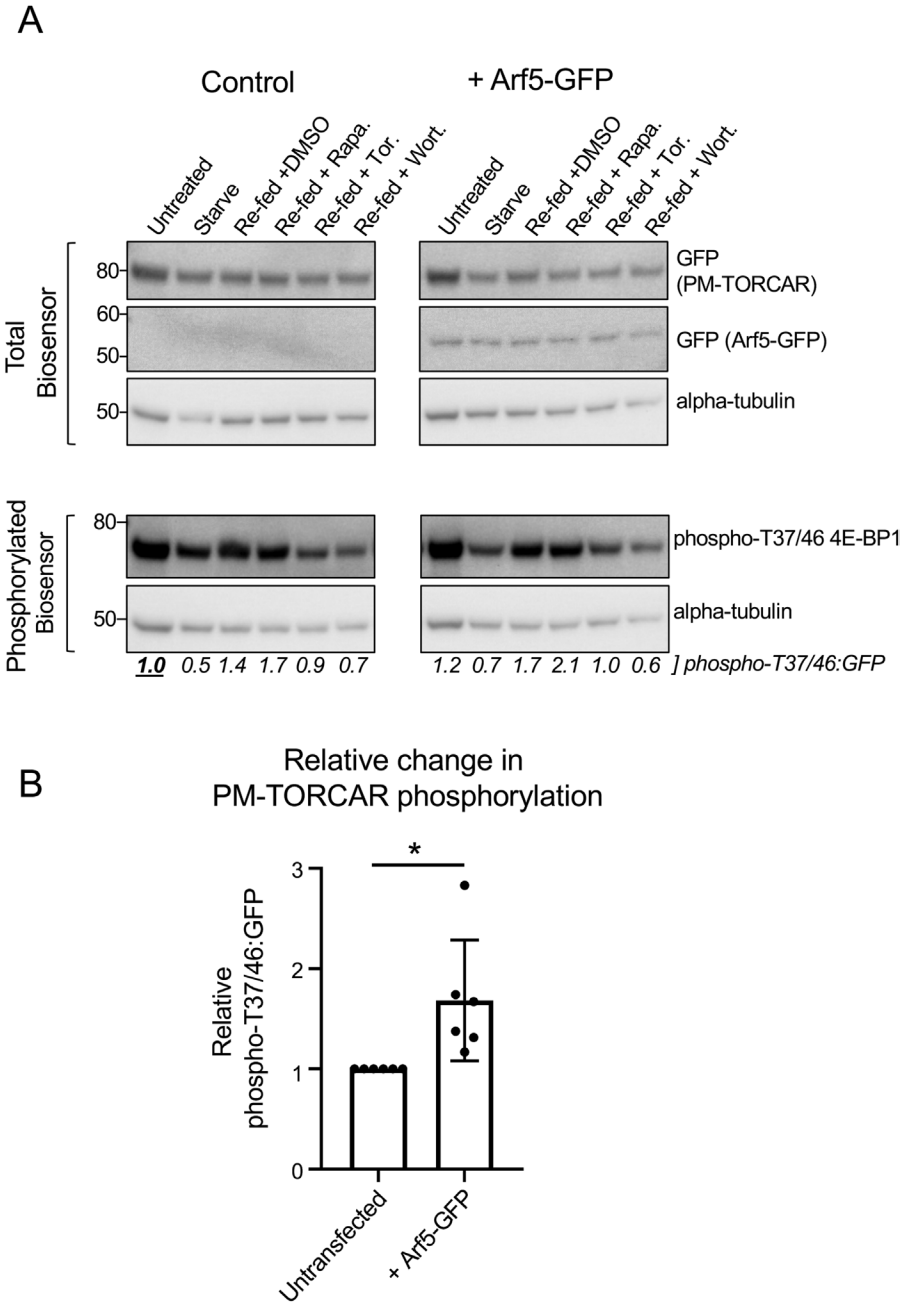

FIGURE 6: Arf5 overexpression enhances PM-TORCAR phosphorylation. (A) HeLa cell monolayers were either transfected with PM-TORCAR alone (control) or cotransfected with Arf5-GFP for 24 h and then starved overnight in serum-free media. Cells were further starved for 2 h in amino acid–free media (EBSS) for 2 h before being refed with complete growth media (C-DMEM) for 45 min in the absence (vehicle) and presence of direct or indirect mTORC1 inhibitors (rapamycin, Torin-1, and wortmannin) as indicated. Cell extracts were identically loaded onto separate protein gels and analyzed by immunoblotting. Using the molecular weight marker as a guide, the PVDF membranes were cut and probed with polyclonal rabbit anti-GFP (total biosensor), rabbit anti–phospho-T37/46 4E-BP1 (phosphorylated biosensor), and α-tubulin. Total and phosphorylated levels of the biosensor were normalized against α-tubulin to give the ratio of phosphorylated to total biosensor (phospho-T37/46:GFP). Changes in phospho-T37/46:GFP are relative to the untreated condition of the untransfected sample. (B) HeLa cells were either transfected with PM-TORCAR alone or cotransfected with Arf5-GFP for 48 h. Cell extracts were analyzed under steady state conditions to determine the phospho-T37/46 4E-BP1:GFP. Data from six independent experiments were pooled to statistically analyze the relative change in phospho-T37/46 4E-BP1:GFP after Arf5-GFP overexpression and are represented as a histogram showing individual values. A paired *t* test was used to analyze the data. $*p < 0.05$. Error bars represent SD.

period (Supplemental Figure S4), whereas the phosphorylation of PM-TORCAR in control cells upon starvation and nutrient replenishment was 70% relative to the prestarved conditions (Supplemental Figure S4). These findings indicate that mTORC1 activation at the PM, as monitored with the biosensor, was severely hindered in Arf5-depleted cells.

To confirm that endogenous Arf5 is essential to regulate mTORC1 activity, HeLa cells were depleted of Arf5, serum and amino acid starved for 2 h, and replenished with complete media for 60 min to stimulate mTORC1 signaling. mTORC1 activity was first assessed by monitoring the changes in phosphorylation of S6, a frequently used reporter of mTORC1 activity that is phosphorylated downstream of mTORC1 activation by ribosomal protein S6 kinase 1 (S6K1) (Chauvin *et al*., 2014). As determined by blotting, Arf5 levels were reduced by >85% in Arf5 siRNA–treated cells compared with control siRNA–treated cells (Figure 8A). Total protein levels of S6 were unaffected by Arf5 depletion or nutrient starvation and replenishment as demonstrated by immunoblotting and normalizing with α-tubulin levels (Figure 8A). Data from four independent experiments showed that S6 phosphorylation levels were reduced by 38.05% ± 0.12 (mean ± SD, $n = 4$) in Arf5-depleted cells under steady state conditions and that starvation resulted in substantial depletion of S6 phosphorylation in both Arf5 siRNA–treated (87.1% reduction) and control siRNA–treated (87.6% reduction) cells (Figure 8, A and B). Following starvation, the recovery of S6 phosphorylation was monitored at 15-min intervals after nutrient enrichment. Analysis of S6 phosphorylation revealed a rapid recovery in control cells, whereas in Arf5-depleted cells there was a reduced level of S6 phosphorylation compared with control siRNA–treated cells (Figure 8). Reduced S6 phosphorylation was particularly pronounced at the 15- and 30-min recovery time points where the average level of phospho-S240/244 S6 was 70 and 50% lower in the Arf5-depleted samples relative to their time point controls (Figure 8B) (15-min time point: Control 0.40 ± 0.06; Arf5 siRNA 0.13 ± 0.05, mean ± SD, $n = 4$; 30-min time point: Control 0.63 ± 0.12; Arf5 siRNA 0.31 ± 0.15, mean ± SD, $n = 4$). We also monitored the phosphorylation of S6K1 in this experiment as it is a direct substrate of mTORC1. The levels of S6K1 phosphorylation under steady state conditions were relatively equal in control and Arf5-depleted HeLa cells. Both samples showed a 75% reduction in S6K1 phosphorylation after serum and amino acid starvation (Supplemental Figure S5, A and B). The recovery of S6K1 phosphorylation was then

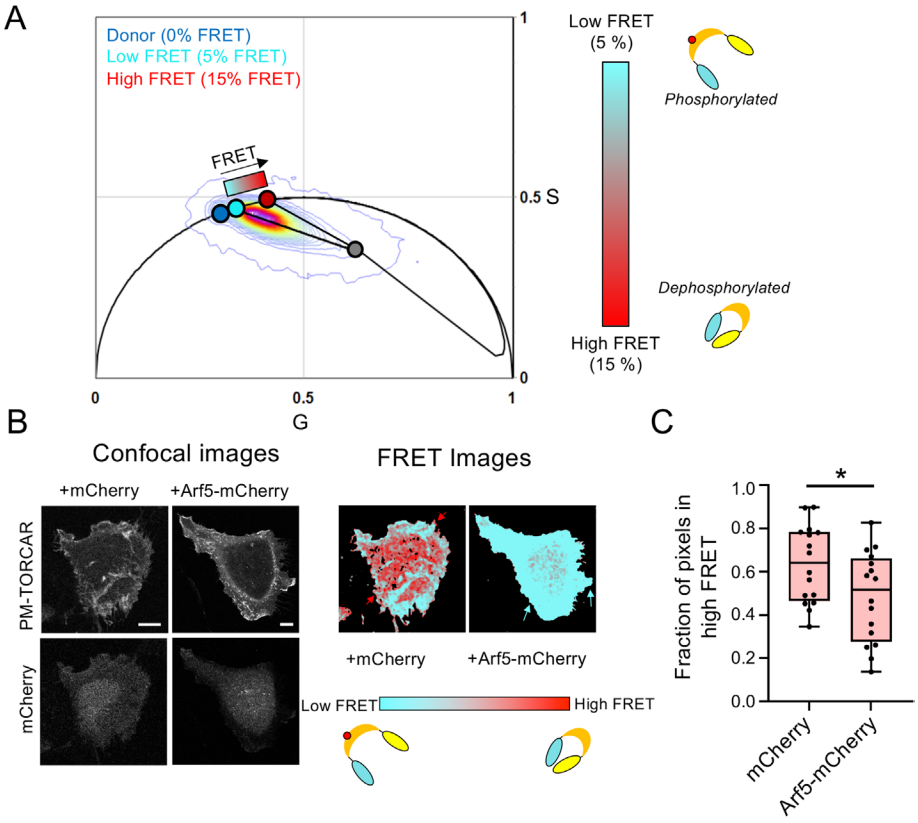

FIGURE 7: FLIM-FRET analysis of PM-TORCAR in Arf5-overexpressing cells. HeLa cell monolayers were cultured in eight-well chamber slides for live-cell imaging and cotransfected with PM-TORCAR and either mCherry or Arf5-mCherry for 24 h as indicated. Cells were then serum starved overnight and amino acid starved for a further 2 h before being refed with C-DMEM for 45 min. Cells were fixed in 4% PFA, quenched in 50 mM ammonium chloride, and kept in PBS. (A) Combined phasor distribution of the Cerulean lifetime for the donor-only control, PM-TORCAR cotransfected with mCherry, and PM-TORCAR cotransfected with Arf5-mCherry. The blue ROI represents the Cerulean lifetime of the donor-only population. The cyan ROI represents the low FRET fraction, and the red ROI represents the high FRET fraction. The background phasor (gray ROI) forms a linear combination with the low FRET state phasor (active biosensor) and high FRET state phasor (inactive biosensor) in each pixel of the FLIM image. The fraction of pixels that are in the low FRET vs. high FRET state for each sample was quantified. (B) Confocal and pseudocolored FRET images of the PM-TORCAR and mCherry or the PM-TORCAR and Arf5-mCherry cotransfected samples. The pseudocolored FRET palette extends from low to high FRET (cyan to red) and enables the spatial distribution of biosensor activity within a given cell to be mapped. Red arrows indicate regions of high FRET, and cyan arrows indicate regions of low FRET. Scale bar = 10 μm. (C) Fraction of pixels (per cell) exhibiting high FRET pooled from two independent experiments; an unpaired *t* test was used to assess significance. $N = 16$ for each sample, $^*p < 0.05$, error bars represent SD.

monitored at 15-min intervals after nutrient enrichment. The phosphorylation of S6K1 at 45 min was significantly lower in Arf5 siRNA–treated samples compared with the control (Supplemental Figure S5); whereas at 15-, 30-, and 60-min intervals there was a reduction in S6K1 phosphorylation in Arf5 siRNA–treated samples, although there was a large variation in the S6K1 phosphorylation levels and the differences were not statistically significant (Supplemental Figure S5). Taken together, these data demonstrated that the loss of Arf5 has a negative impact on the mTORC1 signaling pathway.

DISCUSSION

A number of intracellular and extracellular cues are sensed by the mTORC1 signaling complex to promote growth and proliferation, including growth factors, nutrients, oxygen levels, energy levels, and stress (Dibble and Manning, 2013). While lysosomes are recognized as a major site for regulation of mTORC1 activation, especially for sensing amino acids and proteins delivered from the extracellular environment (Saxton and Sabatini, 2017), there is emerging evidence that mTOR can be activated from additional distinct pools or hubs in the cell and that spatial regulation of mTOR plays an important role in fine-tuning mTORC1 signaling (Gosavi *et al.*, 2018; Rabanal-Ruiz *et al.*, 2021). Our findings presented here extend the identification of the mTORC1 signaling hubs by growth factors and nutrients and provide a mechanism for the delivery of mTORC1 to the PM for activation. Using Raptor as a bait protein, we have identified a role for the small G protein Arf5 as a novel interactor with Raptor and demonstrated the functional importance of this interaction for mTORC1 localization and activation at the plasma membrane. Our findings demonstrate that increased expression of Arf5, or EGF activation, enhances mTORC1 activity at the plasma membrane and that depletion of Arf5 led to 1) a reduction of mTORC1 at peripheral ruffles and 2) retarded mTORC1 activation in response to serum and amino acid enrichment. Overall, our study shows that endogenous Arf5 promotes the recruitment of endogenous mTORC1 to membrane ruffles for activation.

Cell surface receptors, for example, insulin receptor and mitogenic receptors, mediate activation of mTORC1 via phosphoinositide-3 kinase (PI3K), yet the potential contribution of a PM pool of mTORC1 has been unclear. A recent report demonstrated that mTORC1 can also be activated at focal adhesions (Rabanal-Ruiz *et al.*, 2021) and the potential for signaling clusters to activate mTORC1 within specific domains at the PM. Arf5 was not detected in the interaction network with mTOR at focal adhesions (Rabanal-Ruiz *et al.*, 2021), suggesting that focal adhesions and membrane ruffling represent distinct pools of mTORC1 and, in addition, that mTORC1 is associated with defined domains at the cell surface that may be regulated by distinct mechanisms.

Arf5 was not identified in previous interactome studies using pull downs and BioID of Raptor (Rahman *et al.*, 2014; Rabanal-Ruiz *et al.*, 2021; Wang *et al.*, 2021). For pull downs, the particular conditions used for the IP are likely to have had an impact on the putative binding partners identified. Also, the previous pull downs used different cell types, which may also account for the difference between analyses (Rahman *et al.*, 2014; Wang *et al.*, 2021). Proximity labeling (BioID) and proteomics using Raptor as the bait did not report Arf5 as an interactor in HeLa cells (Rabanal-Ruiz *et al.*, 2021). However, BioID labeling efficiency will determine which potential partners are identified, and studies from our lab comparing proximity labeling and pull downs of the same bait (Arl5b) showed that the pull downs detected

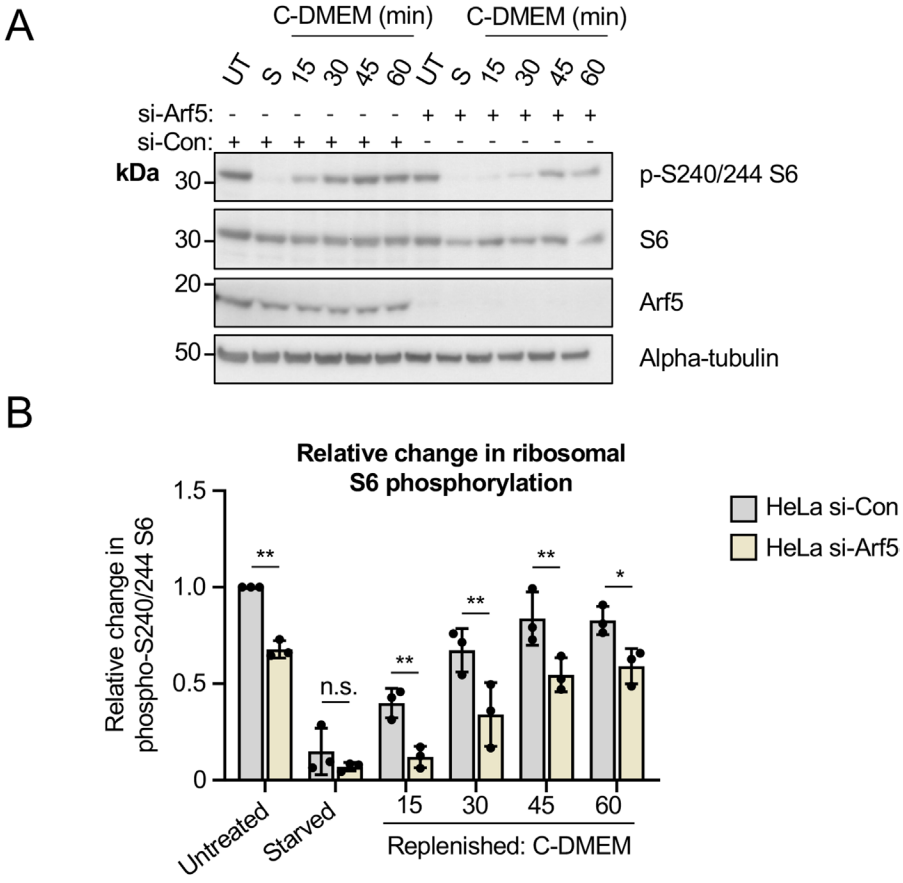

FIGURE 8: Arf5 depletion impairs mTORC1 activation. (A) HeLa cell monolayers were treated with either control or Arf5 siRNA for 72 h. Cells were serum and amino acid starved in EBSS for at least 2 h and refed in complete growth media (C-DMEM) for 60 min. Cells extracts were harvested and analyzed by immunoblotting. Using the molecular weight marker as a guide, the PVDF membrane was cut and probed with antibodies to p-S240/244 S6, Arf5, and α-tubulin as indicated. Images were developed using a chemiluminescence system. Phospho blots were then stripped and reprobed for S6, as indicated, to analyze the total level of substrate. (B) S6 phosphorylation levels were normalized against α-tubulin, and the relative changes from three independent experiments were pooled and analyzed using a two-way ANOVA coupled with Sidak's multiple comparison test. n.s. = not significant, $*p < 0.05$, $**p < 0.01$. Error bars represent SD.

proteins that were not detected in the proximity labeling procedures (Houghton *et al.*, 2022). Hence, there are probably a number of reasons why Arf5 had not been detected in earlier proteomic studies.

The activation of mTORC1 at PM ruffles appears to be lysosome independent, as we showed that mTOR at PM ruffles is spatially distinct from CD63-positive lysosomes in the cell periphery and that the biosensor substrate PM-TORCAR was phosphorylated at the PM. The study by Rabanal-Ruiz *et al.* (2021) also demonstrated that lysosomes are not required for activation of mTORC1 targeted to focal adhesions.

Rheb GTPase is a known factor for activation of mTORC1, and our findings showed that Rheb GTPase was tightly associated with mTORC1-positive membrane ruffles. Arf5-mediated regulation of mTORC1 responses from these membrane ruffles was associated with S6 phosphorylation, S6K phosphorylation, and 4E-BP1 phosphorylation, demonstrating that the activation of mTORC1 at the cell surface promotes downstream signaling. However, at this stage the downstream pathways promoted by mTORC1 signaling from membrane ruffles have yet to be identified.

Arf5 is expressed at varying levels within all tissues (Lebeda *et al.*, 1999) and is also localized to a number of different compartments in addition to the plasma membrane (Chun *et al.*, 2008; Hasegawa *et al.*, 2012; Sukhanova *et al.*, 2013; Kulasekaran *et al.*, 2021). While Arf5 has not been previously documented to regulate mTORC1, other members of the Arf small G protein family, namely Arf1 and Arf4, have been shown to influence mTORC1 activity through independent mechanisms (Li *et al.*, 2010; Jewell *et al.*, 2015; Rainero *et al.*, 2015). For example, Jewell *et al.* (2015) showed that Arf1 is required for RagA/B-independent mTORC1 translocation and activation at the lysosomes in response to glutamine stimulation, whereas other reports have suggested that Arf1 overexpression suppressed mTORC1 signaling specifically in response to amino acid stimulation (Li *et al.*, 2010). Hence, members of the Arf GTPase family may play a major role in mTORC1 activation at different locations.

Our data support a functional interaction between Arf5 and Raptor at membrane ruffles. Membrane ruffles are dynamic membrane protrusions that are characterized as nonadhesive structures that form vertical extensions such as lamellipodia (peripheral ruffles), filopodia (dorsal ruffles), or circular dorsal ruffles (CDRs) (Hoon *et al.*, 2012; Innocenti, 2018). Membrane ruffles regulate a range of cellular processes including directed migration, cell adhesion, and fluid-phase uptake (Mellstrom *et al.*, 1988; Sero *et al.*, 2011), and all of these PM-mediated processes have been shown to interact with the mTORC1 signaling pathways (Chen *et al.*, 2015; Charpentier *et al.*, 2020).

By analyzing the phosphorylation of the downstream mTORC1 ribosomal protein S6 and the biosensor PM-TORCAR, overexpression of wild-type Arf5 led to a significant increase in PM-TORCAR phosphorylation. The Arf5-mediated increase in PM-TORCAR phosphorylation was shown to be mediated by mTORC1 as Torin-1 and wortmannin inhibited this increased phosphorylation of the surrogate substrate. These data strongly suggest that Arf5 regulates the recruitment and activation of mTORC1 to peripheral ruffles through either a direct or an indirect interaction with Raptor. The depletion of Arf5 in HeLa cells was shown to reduce steady state mTORC1 activity and to retard mTORC1 activation following starvation and nutrient refeeding, suggesting that PM-localized mTORC1 plays an important role in the kinetics of mTORC1 activation by nutrient stimuli. As Arf5 knockdown reduced, but did not eliminate, mTORC1 at the plasma membrane, additional factors are likely to contribute to plasma membrane recruitment of mTORC1.

Wild-type and GDP-bound (T31N) Arf5 coprecipitated with myc-Raptor. Although the GTP-bound forms of the small G proteins are typically associated with functional activities, there have been other reports of GDP Arf variants involved in the regulation of a variety of cellular process. Of relevance is that Hasegawa *et al.* (2012) found that overexpression of the GDP-bound form (T31N) of Arf1 or Arf5

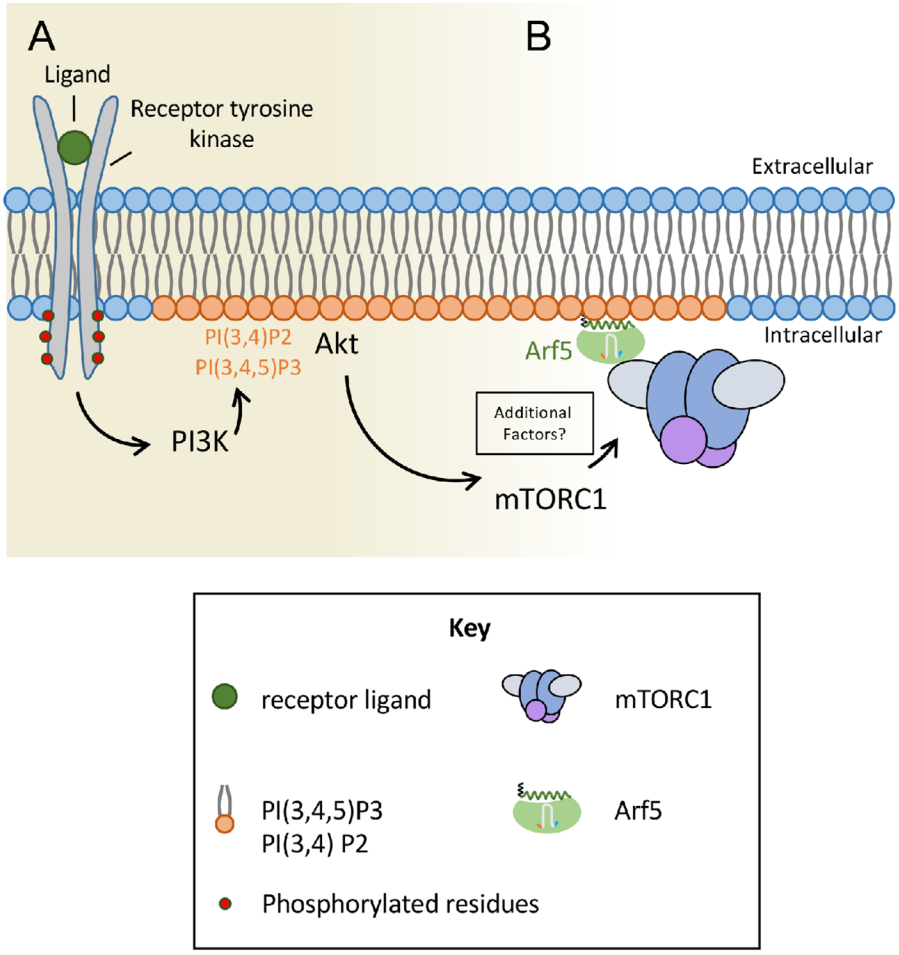

FIGURE 9: Proposed model for Arf5-mediated recruitment of mTORC1 to membrane ruffles. (A) Tyrosine kinase receptor ligand binding leads to the activation of the PI3K/Akt/mTOR pathway and then the generation of PI(3,4,5)P3 and PI(3,4)P2. Akt is recruited to PI(3,4,5)P3/PI(3,4)P2-rich membranes through its PH domain and activated at the PM. mTORC1 is activated by Akt; (B) the model proposes that membrane-bound Arf5 promotes the recruitment of mTORC1 to the PI-rich membrane ruffles to facilitate its activation through the PI3K/Akt signaling pathway. The mechanism for membrane association of Arf5 with the PM is unknown.

led to an increase in the size of CDRs. Also, GDP-bound Arf4 and Arf5 have been shown to be recruited to the Golgi to regulate anterograde transport through an interaction with the PH domain of CAPS1 (Ca^{2+}-dependent activator protein for secretion) (Sadakata *et al.*, 2010). Hence, these previous findings are compatible with our observation that GDP-bound Arf5 is recruited to the PM and could regulate a membrane-mediated process.

On the basis of our findings reported in this article, together with the activities of other small GTPases, we propose a model whereby peripheral ruffles mediate the membrane association Arf5, which in turn then recruits mTORC1 to the PM through its interaction with Raptor (Figure 9). The recruitment of mTOR to membrane ruffles would facilitate the activation of mTORC1 via the PI3K/Akt pathway following receptor activation (Figure 9). Such a mechanism would provide a very rapid activation of mTORC1 and may also influence the subsequent substrates for mTORC1 phosphorylation. Further work is now required to determine whether the location and activation of mTORC1 on membrane ruffles regulate selective downstream responses.

MATERIALS AND METHODS

Request a protocol through *Bio-protocol*.

siRNA duplexes

The predesigned siRNA target sequences (Table 1) were purchased from Sigma-Aldrich.

Plasmids

pcDNA3-PM-TORCAR and pcDNA3-Lyso-TORCAR (Addgene plasmids #64930 and #64929) were a kind gift from Jin Zhang (Zhou *et al.*, 2015). pRK-5-Myc-Raptor was a kind gift from David Sabatini (Addgene plasmid #1859) (Sarbassov *et al.*, 2004). pcDNA3-hArf5(WT)-mCherry and pEGFP-N3-hArf5(WT)-EGFP were a kind gift from Kazuhisa Nakayama (Kyoto University, Japan; Addgene plasmids #79421 #79534) (Kondo *et al.*, 2012; Makyio *et al.*, 2012). pcDNA3-hArf5(WT)-HA, pcDNA3-hArf5(Q71L)-HA, and pcDNA3-hArf5(T31N)-HA (Addgene plasmids #79427, #79428, and # 79429, respectively, were a kind gift from Kazuhisa Nakayama (Hanai *et al.*, 2016). pRK5myc-Rab6A(Q72L) was a kind gift from Bruno Goud (Curie Institute, Paris) (Beranger *et al.*, 2002).

Constructs

To generate a donor-only control for the plasma membrane targeted mTOR biosensor, the primers 5′-TAAGAATTCTGCAGATATCC-3′ and 5′-GAATTCCTAAATGTCCATCTCAAACTG-3′ were used to amplify pcDNA3-PM-TORCAR, which excluded base pairs 3262–3981 and which encoded YFP. These primers introduced 3′ and 5′ *Eco*RI restriction sites into the final product and a stop codon following the 4E-BP1 sequence. *Eco*RI sites were used to self-ligate the 3′ and 5′ ends of the PCR product, which gave rise to a plasma membrane–targeted donor-only control (Lyn-CFP-4E-BP1).

mCherry-TAPP1-C-PH was previously generated as described (Lim *et al.*, 2008). The C-terminal PH domain of TAPP1 (aa 95–400) targets this protein to the plasma membrane and is conjugated to mCherry to serve as a marker for the plasma membrane.

Arl5b(Q70L)-BirA(R118G)-HA: Arl5b(Q70L) was amplified from pEGFP-Arl5b(Q70L) (Houghton *et al.*, 2012) using the primers 5′-CCGGAATTCCGGACCATGGGGCTGATCTTC-3′ and 5′-CGCGGATCCGCGTCTCACACCAATCCG-3′, which introduced *Eco*R1

Target	Sequence (5′-3′)
Arf5	CUCAUCUUUGUGGUGGACA
mTOR	CUAGUGAAAUGCUGGUCAA
Raptor	CUAGUCUGUUUCGAAAUUU
Rheb	CAAACUGCCCGUUCUCCUU
Control	AAGUCGGUGUGCUCUUGUUGG

TABLE 1: siRNA target sequences.

and *Bam*HI in-frame with Arl5b(Q70L). The PCR product was digested with *Eco*RI/*Bam*HI and subcloned into the pcDNA3.1-BirA(R118G)-HA vector digested with *Eco*R1/*Bam*HI to create pcDNA3.1-Arl5b(Q70L)-BirA(R118G)-HA.

Antibodies and conjugates

Rabbit polyclonal antibodies to human GCC88 have been described (Luke *et al*., 2003). Mouse monoclonal antibodies to human golgin-97 (#CDF4 A-21270;1:600) and GM130 (#610882; 1:600) were purchased from BD Biosciences (Australia). Human autoantibodies to golgin-245 (p230) have been described (Kooy *et al*., 1992). Mouse monoclonal antibodies to GAPDH were purchased from Calbiochem (#MAP374; 1:5000). Rabbit polyclonal antibodies to Vps26 (#ab23892; 1:200), myc-tag (9B11) (#ab9106; 1:2000), golgin-97 (#ab84340; 1:400), GFP (#ab6556; 1:1000), mouse monoclonal antibody against Rheb (#ab97896; 1:500), and rabbit monoclonal antibody against Raptor (#ab26264; 1:500) were purchased from Abcam, UK. Mouse monoclonal antibody to myc-tag (clone 9B11) (#2276S; 1:1000) was purchased from NEB, USA. Mouse monoclonal antibody to α-tubulin (clone DM1A) (#T9026; 1:5000), FLAG (clone M2) (#F3165; 1:1000), Arf5 (#WH0000381M1; 1:500), and rabbit polyclonal antibodies to FLAG (#F7425 1:2000) were obtained from Sigma-Aldrich. Phalloidin-tetramethylrhodamine B isothiocyanate (phalloidin-TRITC) (#P1951; 1:2000; Sigma-Aldrich) was used to detect actin filaments. Mouse monoclonal antibodies to GFP (clone 7.1 and 17.1) (#11814460001; 1:1000) were purchased from Roche Applied Science, Germany. Rabbit polyclonal antibodies to mTOR (#2983; 1:500), phospho-Ser240/244 S6 (#2217; 1:500), p70 S6 kinase (#9202; 1:500), phospho-Thr389 p70 S6 kinase (#9205; 1:500), phospho-Thr37/46 4E-BP1 (#2855; 1:500), HA-tag (clone C29F4) (#3724; 1:1000), and rabbit monoclonal antibodies against ribosomal protein S6 (clone 5G10) (#2217; 1:500), 4E-BP1 (#9644; 1:500), and PRAGC/RagC (clone D8H5) (#9480S; 1:500) were purchased from Cell Signalling Technologies, Australia. Rabbit polyclonal antibody against GFP (PABG1; 1:500) was from ChromoTek, Germany. Mouse monoclonal antibody against HA-tag (clone 16B12) (#MMS-101R; 1:1000) was purchased from Covance, USA. Mouse monoclonal antibodies against EGFR (clone A-10) (#sc-373746; 1:500) and CD63 (#sc5275; 1:1500) were purchased from Santa Cruz, USA.

Secondary antibodies used for immunofluorescence were goat anti-rabbit immunoglobulin G (IgG)–Alexa Fluor 568, goat anti-mouse IgG–Alexa Fluor 568, goat anti-rabbit IgG–Alexa Fluor 488, goat anti-mouse IgG–Alexa Fluor 488, goat anti-mouse IgG–Alexa Fluor 647, goat anti-rabbit IgG–Alexa Fluor 647, and goat anti-human Alexa Fluor 568 or 647 were from Life Technologies (Grand Island, NY). All secondary antibodies were used at the dilution 1:500. Horseradish peroxidase–conjugated rabbit anti-goat Ig, horseradish peroxidase–conjugated sheep anti-rabbit Ig, and anti-mouse Ig were from DAKO Corporation (Carpentaria, CA). Streptavidin–Alexa Fluor 488 and streptavidin–horseradish peroxidase were purchased from Life Technologies (USA).

Cell culture and transfection

Mycoplasma-free, authentic, HeLa cells (Curie Institute, Paris), verified by genomic sequencing, and RAW264.7 cells (Ralph and Nakoinz, 1977) were maintained as semiconfluent monolayers in DMEM (Thermo Fisher Scientific, Australia) supplemented with 10% fetal bovine serum (FBS) (Life Technologies, Australia), 100 U/μl penicillin and 0.1% (wt/vol) streptomycin (complete DMEM [C-DMEM]) in a humidified 10% CO_2 atmosphere at 37°C. Cells were routinely tested for mycoplasma contamination using the MycoAlert Mycoplasma Detection Kit (Lonza, Switzerland).

Transient transfections of DNA plasmids and siRNA

Transient transfections of DNA plasmids were performed using the FuGENE 6 transfection reagent (Promega, USA), Lipofectamine 2000, or Lipofectamine 3000 (Thermo Fisher Scientific, Australia) according to the manufacturer's protocol. Transfection of siRNA sequences was performed using DharmaFECT1 (GE Lifesciences/Millennium Science, Australia) or Lipofectamine 3000 (Thermo Fisher Scientific, Australia) according to the manufacturer's protocol for 72 h before analysis.

Nutrient deprivation and replenishment with complete growth media

Nutrient deprivations and replenishment were used to monitor mTORC1 activity by analyzing the phosphorylation of its downstream substrates. For analysis of endogenous substrates, cells were washed twice with sterile phosphate-buffered saline (PBS) and serum and amino acid starved in Earle's balanced salt solution (EBSS) (cat #24010043; Thermo Fisher Scientific, Australia) for 1–2 h. Cells were then incubated in C-DMEM for the indicated time and processed for analysis.

To pharmacologically inhibit mTORC1 activity, cells were amino acid starved for 2 h in EBSS that was supplemented with one of the following inhibitors: 2.5 μM Torin-1 (#14379; Cell Signalling Technologies), 10 μM wortmannin (#W1628; Sigma-Aldrich), or 50 nM rapamycin (#9904S; Cell Signalling Technologies). Torin-1, wortmannin, and rapamycin were then diluted to the same final concentrations in C-DMEM, and cells were nutrient replenished in the presence of mTORC1 inhibitors for the indicated time. Control cells were replenished with C-DMEM that was supplemented with dimethyl sulfoxide (DMSO) instead of the inhibitors.

For nutrient deprivation with TORCAR variants, cells were seeded at 0.4×10^5/well or 0.96×10^5/well in 12- or 6-well plates, respectively, and incubated overnight in C-DMEM. Cells were transfected with the TORCAR biosensor variant for 24 h using FuGENE 6 according to the manufacturer's recommendations. To dephosphorylate the biosensor, the cells were washed twice in sterile PBS and incubated in serum-free media (i.e., DMEM) for 24 h. Samples were washed again with sterile PBS and amino acid starved in EBSS for 2 h. To monitor the recovery of TORCAR phosphorylation, EBSS was replaced with C-DMEM for the indicated time and the cells were processed accordingly.

EGF stimulation

Cell cultures were washed twice with PBS and then serum starved in DMEM for ~16 h. Cells were then treated with 25 ng/ml hEGF recombinant protein (#PHG0311L; Life Technologies, Australia) in DMEM for the indicated time and processed accordingly for further analysis.

Indirect immunofluorescence microscopy

Monolayers on coverslips were fixed with 4% (vol/vol) paraformaldehyde (PFA) for 15 min, followed by quenching in 50 mM NH_4Cl/PBS for 10 min. Cells were permeabilized in 0.1% Triton X-100 in PBS for 4 min and incubated in 5% FBS in PBS for 20 min to reduce nonspecific binding. Monolayers were incubated with primary antibodies diluted in 5% FBS/PBS for at least 1 h at room temperature and then extensively washed in PBS. Secondary conjugates were also diluted in 5% FBS/PBS and incubated with the cell monolayers for at least 1 h before being washed extensively in PBS with a final wash in

MilliQ. Coverslips were mounted in mowiol containing 4,6-diamidino-2-phenyindole (DAPI).

Confocal microscopy

Images were acquired using a laser confocal scanning microscope (Leica LCS SP8 confocal imaging system) using a 63× 1.4 NA HCX PL APO CS oil immersion objective. YFP, GFP, and Alexa Fluor 488 were excited with the 488-nm solid-state laser (SSL), Alexa Fluor 568 with a 552-nm SSL, Alexa Fluor 647 with a 638-nm SSL, and DAPI with a 405-nm diode laser. Images were collected sequentially for multicolor imaging. Fluorescence images for each experiment were collected using identical settings. Scale bars were added using ImageJ software.

Superresolution imaging

Images were acquired using a laser confocal scanning microscope (ZEISS LSM 880 with Airyscan) equipped with a 63× 1.4 NA Plan-Apochromat (420782-9900-799) oil immersion objective and 32 hexagonal array Airyscan detector. Images were acquired using the fast Airyscan mode. Alexa Fluor 488 was excited with the 488-nm SSL, Alexa Fluor 568 with a DPSS 561-nm (10 mW) laser, and DAPI with a 405-nm diode laser. Images were collected sequentially for multicolor imaging. Fluorescence images for each experiment were collected using identical settings. Huygens deconvolution software was used to deconvolute the raw image files using a conservative setting. Scale bars were added after deconvolution using ImageJ software.

Quantitation of the fluorescence within a masked region

ImageJ was used to generate a mask for the region of interest (ROI), which was used to quantify the MFI of a fluorescence signal within this ROI. The data were then exported to GraphPad Prism for statistical analysis.

Line scan analysis

Line spectrum reports were generated for a ROI using LAS X Life Science microscope software and exported into Excel, which was used to construct the line graphs.

FLIM and phasor analysis

Cell monolayers were cultured in an eight-well μ-slide (iBidi; cat# 80826) and transfected with the desired biosensor. Cells were fixed with 4% (vol/vol) PFA for 15 min, followed by quenching in 50 mM NH_4Cl/PBS for 10 min. Fixed cells were then extensively washed and stored in PBS. Cells were imaged in PBS, and fluorescence lifetime measurements were collected within 24 h of fixing the cells.

All FLIM measurements of FRET were performed on an Olympus FV3000 laser scanning microscope coupled to a 440-nm pulsed laser operated at 80 MHz and an ISS A320 FastFLIM box for time-resolved detection. To confirm the presence of the single chain biosensor in the transfected cells, an intensity image of the donor localization was first acquired via the use of an internal solid-state laser diode operating at 488 nm, a 405/488/561 dichroic mirror, and an internal GaAsP photomultiplier detector set to collect the 490–560 nm bandwidth. A FLIM image (20 μs/pixel, 15 frame integration, 512 × 512 or 256 × 256 pixel frame size) was then acquired of the single chain biosensor via the use of an external 440 nm pulsed laser (80 MHz), and the resulting fluorescence signal was directed through a 440 nm dichroic mirror to an external photomultiplier detector (H7422P-40; Hamamatsu) fitted with a 480/50 nm bandwidth filter. The FLIM image of the biosensor was processed by the ISS Vista Vision software that precalibrates the instrument and phasor space using a known reference lifetime (fluorescein at pH 9.0, 4.04 ns lifetime).

FLIM-FRET data were analyzed in the SimFCS software developed at the Laboratory for Fluorescence Dynamics, as described (Digman *et al.*, 2005; Hinde *et al.*, 2012). The fluorescence lifetime that was recorded in each pixel of a FLIM-FRET image is described by a G and S coordinate (phasor) in the phasor plot. In pixels where the donor undergoes FRET with an acceptor molecule, the phasor coordinate will be right shifted along a curved trajectory that is described by the classical definition of FRET efficiency. The experimental position of the phasor of a given pixel along the trajectory determines the FRET efficiency of that location. Because the TORCAR biosensor is a single chain design that gives rise to a low and a high FRET state (Hinde *et al.*, 2012), phasor cursors were defined to detect these two states and then used to spatially map TORCAR biosensor activity throughout a single cell and quantify the fraction of pixels exhibiting mTOR1 phosphorylation across multiple cells.

Immunoblotting

Cells were lysed in RIPA buffer (1 mM Tris/Cl, pH 7.5, 15 mM NaCl, 0.5 mM EDTA, 0.01% SDS, 0.1% Triton X-100, and 0.1% deoxycholate) containing protease inhibitors (Sigma-Aldrich, Australia) and phosphatase inhibitors (PhosSTOP; #4906845001; Sigma-Aldrich, Australia). Aliquots of the extracts were added to reducing SDS sample buffer and boiled for 8 min at 100°C. Proteins were resolved by SDS–PAGE using 4–12% NuPAGE gels and transferred onto an Immobilon-P polyvinylidene fluoride (PVDF) membrane (Millipore, Australia) at 30 V overnight at 4°C. The membrane was blocked by drying at 37°C and then rehydrated in 0.1% (vol/vol) PBS-Tween 20. The membrane was incubated with antibodies diluted in 5% (wt/vol) skim milk in PBS, either at room temperature for 1 h or overnight at 4°C, and then washed three times, each for 10 min, in 0.1% (vol/vol) PBS-Tween 20. The PVDF membrane was then incubated with horseradish peroxidase–conjugated secondary antibodies, diluted in 5% (wt/vol) skim milk in PBS for 1 h and washed as above.

Immunoblotting using phosphospecific antibodies or antibodies purchased from cell signaling technology (Australia) was performed with the following changes. The PVDF membrane was rehydrated in 0.1% (vol/vol) TBS-Tween 20 and blocked in 1% bovine serum albumin (BSA)/0.1% (vol/vol) TBS-Tween 20 for 1 h at 4°C with gentle agitation. The membrane was incubated with antibodies diluted in 5% (wt/vol) BSA in 0.1% (vol/vol) TBS-Tween 20 overnight at 4°C and then washed three times, each for 10 min, in 0.1% (vol/vol) TBS-Tween 20. The PVDF membrane was then incubated with horseradish peroxidase–conjugated secondary antibodies, diluted in 5% (wt/vol) BSA in 0.1% (vol/vol) TBS-Tween 20 for 1 h and washed as above. Bound antibodies were detected by enhanced chemiluminescence (Amersham, GE Healthcare, Australia) and captured using Gel-Pro Analyser version 4.5 software (MediaCybernetics, Berthesda, MD) or the Chemi-Doc MP imager system (Bio-Rad). Band intensities were quantified using Image Lab software (Bio-Rad) and exported into Excel or GraphPad Prism for statistical analysis.

myc-Raptor immunoprecipitation

Three 100 mm plates were prepared for each sample, with 1.0×10^6 HeLa cells seeded into each plate and cultured overnight. Cells were transfected with myc-Raptor or myc-Rab6A(Q72L), as control, using FuGENE6 (Promega, USA) according to the manufacturer's protocol. Cells were harvested by trypsinization, washed twice in chilled PBS, and lysed in cell lysis buffer (50 mM HEPES, 40 mM NaCl, 2 mM EDTA, 1% [vol/vol] Triton X-100, 1× protease inhibitor, and 1× phosphatase inhibitor in MilliQ) for 30 min on ice. Lysates were

centrifuged at 15,000 × *g* for 15 min at 4°C, and the supernatant was transferred to a fresh 1.5 ml tube. Ten percent of the volume was kept aside as input reference. Dynabeads Protein G (Thermo Fisher Scientific, Australia) were washed twice, initially in 0.1% TBS-T (5% FBS in Tris-buffered saline (TBS) containing 0.1% Tween 20), followed by cell lysis buffer, after which the beads (20 µl) were used to preclear the cell lysates for 1 h at 4°C. In a separate tube, mouse anti-myc (9E10) antibody was incubated with Dynabeads Protein G for 1 h at 4°C and the beads were washed to remove any unbound antibody. Precleared lysates were then incubated overnight at 4°C with Dynabeads Protein G bound to mouse anti-myc antibody. The beads were washed a total of six times, once in each of the following buffers: wash buffer 1.0 (0.05% Tween 20 in TBS), wash buffer 1.1 (50 mM HEPES, 40 mM NaCl, 2 mM EDTA, and 1× protease/phosphatase inhibitor), wash buffer 1.2 (50 mM HEPES, 40 mM NaCl, 2 mM EDTA, 1× protease/phosphatase inhibitor, 1% [vol/vol] Triton X-100), wash buffer 1.3 (50 mM HEPES, 40 mM NaCl, 2 mM EDTA, 1× protease/phosphatase inhibitor, 0.5% [vol/vol] Triton X-100, 500 mM LiCl), wash buffer 1.4 (50 mM HEPES, 40 mM NaCl, 2 mM EDTA, 1× protease/phosphatase inhibitor, 500 mM LiCl), and wash buffer 1.5 (50 mM HEPES, 150 mM NaCl, 1× protease/phosphatase inhibitor). For immunoblotting analysis, the beads were boiled in 4× SDS sample reducing buffer for 8 min at 100°C. Bead/protein complexes were processed for mass spectrometry analysis.

In-solution trypsin digestion and mass spectrometry

To identify anti-myc immunoprecipated proteins by mass spectrometry, Dynabead/protein complexes from above were washed with 100 µl of 1 mM triethylammonium bicarbonate (TEAB) and centrifuged at maximum speed for 5 min. One microliter of 2,2,2-trifluoroethanol (TFE), 1 µl of 0.1% formic acid, and 5 µl of MilliQ were then added to the beads and briefly incubated. Proteins were reduced in 2 mM *tris* 2-carboxyethylphosphine (TCEP) in 10 mM TEAB (pH 8.5) and then alkylated in the dark with 55 mM iodoacetamide in 50 mM TEAB for 30 min. The samples were centrifuged for 5 min at maximum speed, and the supernatant was transferred to a fresh tube. Eluted proteins were digested overnight with 0.25 µg of trypsin (trypsin singles, proteomics grade; Sigma-Aldrich) at 37°C. Samples were then centrifuged for 5 min at maximum speed, transferred to a fresh MS tube, and analyzed by mass spectrometry. The proteins that were identified in the myc-Rab6A(Q72L) control, based on two unique peptide matches, were subtracted from the myc-Raptor. Proteins were further filtered in the myc-Raptor sample to contain at least three unique peptide matches. A protein was designated as a candidate interactor of Raptor if it exclusively appeared in at least two independent experiments.

Mass spectrometry

Samples were analyzed on a LTQ Orbitrap Elite (Thermo Scientific) coupled to an Ultimate 3000 RSLC nanosystem (Dionex). The nanoLC system was equipped with an Acclaim Pepmap nano-trap column and an Acclaim Pepmap analytical column. The peptide mix (2 µl) was loaded onto the trap column at 3% acetonitrile containing 0.1% formic acid for 5 min before the enrichment column was switched in-line with the analytical column. The LC gradient was 3–25% acetonitrile over 20 min and then 40% acetonitrile for 2 min (total run time was 38 min). The LTQ Orbitrap Elite mass spectrometer was operated in the data-dependent mode, spectra acquired first in positive mode at 240k resolution followed by collision-induced dissociation (CID) fragmentation. Twenty of the most intense peptide ions with charge states ≥2 were isolated per cycle and fragmented using normalized collision energy of 35 and activation Q of 0.25 (CID).

Data analysis was carried out using the Mascot protein identification search engine (Matrix Science; v2.4) and restricted to the SWISSPROT database. Search parameters used were a 10 ppm peptide mass tolerance and 0.6 Da fragment ion mass tolerance. Carbamidomethyl (C) was set as a fixed modification, and oxidation (M) was included as a variable modification. Three missed cleavages were permitted, and the search taxonomy was restricted to *Homo sapiens*. Peptides with a Mascot ion score greater than the homology score were considered significant.

Bioinformatic analysis of myc-Raptor–interacting proteins

The membrane localization of the identified proteins in the myc-Raptor immunoprecipitates was determined using the GO cellular compartments database and proteins that were strictly localized to the nucleus or only to the nucleus, and the cytosol was excluded from farther-downstream analysis. A pie chart was used to represent the distribution of protein hits throughout the cell. Proteins that are localized to more than one subcellular compartment were reported as such. Myc-Raptor candidate interacting partners were analyzed via STRING analysis to identify previously characterized interactors of Raptor.

Statistical analysis

All statistical analysis was performed using GraphPad Prism software as indicated in the relevant figure legends.

ACKNOWLEDGMENTS

Confocal microscopy was performed at the Biological Optical Microscopy Platform (BOMP), University of Melbourne, and mass spectrometry in the Bio21 Mass Spectrometry and Proteomics Facility (MSPF) at the Bio21 Molecular Science and Biotechnology Institute, University of Melbourne. This work was supported by funding from the Australian Research Council (DP160102394).

REFERENCES

Angarola B, Ferguson SM (2019). Weak membrane interactions allow Rheb to activate mTORC1 signaling without major lysosome enrichment. Mol Biol Cell 30, 2750–2760.

Angarola B, Ferguson SM (2020). Coordination of Rheb lysosomal membrane interactions with mTORC1 activation. F1000Res 9, F1000 Faculty Rev-450.

Bar-Peled L, Schweitzer LD, Zoncu R, Sabatini DM (2012). Ragulator is a GEF for the rag GTPases that signal amino acid levels to mTORC1. Cell 150, 1196–1208.

Beranger F, Mange A, Goud B, Lehmann S (2002). Stimulation of PrP(C) retrograde transport toward the endoplasmic reticulum increases accumulation of PrP(Sc) in prion-infected cells. J Biol Chem 277, 38972–38977.

Betz C, Hall MN (2013). Where is mTOR and what is it doing there? J Cell Biol 203, 563–574.

Brown EJ, Albers MW, Shin TB, Ichikawa K, Keith CT, Lane WS, Schreiber SL (1994). A mammalian protein targeted by G1-arresting rapamycin-receptor complex. Nature 369, 756–758.

Buerger C, DeVries B, Stambolic V (2006). Localization of Rheb to the endomembrane is critical for its signaling function. Biochem Biophys Res Commun 344, 869–880.

Chao LH, Avruch J (2019). Cryo-EM insight into the structure of MTOR complex 1 and its interactions with Rheb and substrates. F1000Res 8, F1000 Faculty Rev-14.

Charpentier JC, Chen D, Lapinski PE, Turner J, Grigorova I, Swanson JA, King PD (2020). Macropinocytosis drives T cell growth by sustaining the activation of mTORC1. Nat Commun 11, 180.

Chauvin C, Koka V, Nouschi A, Mieulet V, Hoareau-Aveilla C, Dreazen A, Cagnard N, Carpentier W, Kiss T, Meyuhas O, Pende M (2014). Ribosomal protein S6 kinase activity controls the ribosome biogenesis transcriptional program. Oncogene 33, 474–483.

Chen L, Xu B, Liu L, Liu C, Luo Y, Chen X, Barzegar M, Chung J, Huang S (2015). Both mTORC1 and mTORC2 are involved in the regulation of cell adhesion. Oncotarget 6, 7136–7150.

Chun J, Shapovalova Z, Dejgaard SY, Presley JF, Melancon P (2008). Characterization of class I and II ADP-ribosylation factors (Arfs) in live cells: GDP-bound class II Arfs associate with the ER-Golgi intermediate compartment independently of GBF1. Mol Biol Cell 19, 3488–3500.

de la Cruz Lopez KG, Toledo Guzman ME, Sanchez EO, Garcia Carranca A (2019). mTORC1 as a regulator of mitochondrial functions and a therapeutic target in cancer. Front Oncol 9, 1373.

Dibble CC, Manning BD (2013). Signal integration by mTORC1 coordinates nutrient input with biosynthetic output. Nat Cell Biol 15, 555–564.

Digman MA, Brown CM, Sengupta P, Wiseman PW, Horwitz AR, Gratton E (2005). Measuring fast dynamics in solutions and cells with a laser scanning microscope. Biophys J 89, 1317–1327.

Donaldson JG, Honda A, Weigert R (2005). Multiple activities for Arf1 at the Golgi complex. Biochim Biophys Acta 1744, 364–373.

Egerer J, Emmerich D, Fischer-Zirnsak B, Chan WL, Meierhofer D, Tuysuz B, Marschner K, Sauer S, Barr FA, Mundlos S, Kornak U (2015). GORAB missense mutations disrupt RAB6 and ARF5 binding and Golgi targeting. J Invest Dermatol 135, 2368–2376.

Fan SJ, Snell C, Turley H, Li JL, McCormick R, Perera SM, Heublein S, Kazi S, Azad A, Wilson C, *et al*. (2016). PAT4 levels control amino-acid sensitivity of rapamycin-resistant mTORC1 from the Golgi and affect clinical outcome in colorectal cancer. Oncogene 35, 3004–3015.

Fourriere L, Cho EH, Gleeson PA (2022). Segregation of the membrane cargoes, BACE1 and amyloid precursor protein (APP) throughout the Golgi apparatus. Traffic 23, 158–173.

Go CD, Knight JDR, Rajasekharan A, Rathod B, Hesketh GG, Abe KT, Youn JY, Samavarchi-Tehrani P, Zhang H, Zhu LY, *et al*. (2021). A proximity-dependent biotinylation map of a human cell. Nature 595, 120–124.

Gosavi P, Houghton FJ, McMillan PJ, Hanssen E, Gleeson PA (2018). The Golgi ribbon in mammalian cells negatively regulates autophagy by modulating mTOR activity. J Cell Sci 131, jcs211987.

Hanai A, Ohgi M, Yagi C, Ueda T, Shin HW, Nakayama K (2016). Class I Arfs (Arf1 and Arf3) and Arf6 are localized to the Flemming body and play important roles in cytokinesis. J Biochem 159, 201–208.

Hao F, Kondo K, Itoh T, Ikari S, Nada S, Okada M, Noda T (2018). Rheb localized on the Golgi membrane activates lysosome-localized mTORC1 at the Golgi-lysosome contact site. J Cell Sci 131, jcs208017.

Hara K, Maruki Y, Long X, Yoshino K, Oshiro N, Hidayat S, Tokunaga C, Avruch J, Yonezawa K (2002). Raptor, a binding partner of target of rapamycin (TOR), mediates TOR action. Cell 110, 177–189.

Hasegawa J, Tsujita K, Takenawa T, Itoh T (2012). ARAP1 regulates the ring size of circular dorsal ruffles through Arf1 and Arf5. Mol Biol Cell 23, 2481–2489.

Hinde E, Digman MA, Welch C, Hahn KM, Gratton E (2012). Biosensor Forster resonance energy transfer detection by the phasor approach to fluorescence lifetime imaging microscopy. Microsc Res Tech 75, 271–281.

Hoon JL, Wong WK, Koh CG (2012). Functions and regulation of circular dorsal ruffles. Mol Cell Biol 32, 4246–4257.

Houghton FJ, Bellingham SA, Hill AF, Bourges D, Ang DK, Gemetzis T, Gasnereau I, Gleeson PA (2012). Arl5b is a Golgi-localised small G protein involved in the regulation of retrograde transport. Exp Cell Res 318, 464–477.

Houghton FJ, Makhoul C, Cho EH, Williamson NA, Gleeson PA (2022). Interacting partners of Golgi-localized small G protein Arl5b identified by a combination of in vivo proximity labelling and GFP-Trap pull down. FEBS Lett 596, 2382–2399.

Innocenti M (2018). New insights into the formation and the function of lamellipodia and ruffles in mesenchymal cell migration. Cell Adh Migr 12, 401–416.

Jewell JL, Kim YC, Russell RC, Yu FX, Park HW, Plouffe SW, Tagliabracci VS, Guan KL (2015). Metabolism. Differential regulation of mTORC1 by leucine and glutamine. Science 347, 194–198.

Kagan JC, Su T, Horng T, Chow A, Akira S, Medzhitov R (2008). TRAM couples endocytosis of Toll-like receptor 4 to the induction of interferon-beta. Nat Immunol 9, 361–368.

Kim LC, Cook RS, Chen J (2017). mTORC1 and mTORC2 in cancer and the tumor microenvironment. Oncogene 36, 2191–2201.

Kondo Y, Hanai A, Nakai W, Katoh Y, Nakayama K, Shin HW (2012). ARF1 and ARF3 are required for the integrity of recycling endosomes and the recycling pathway. Cell Struct Funct 37, 141–154.

Kooy J, Toh BH, Pettitt JM, Erlich R, Gleeson PA (1992). Human autoantibodies as reagents to conserved Golgi components—characterization of a peripheral, 230-kDa compartment-specific Golgi protein. J Biol Chem 267, 20255–20263.

Kulasekaran G, Chaineau M, Piscopo VEC, Verginelli F, Fotouhi M, Girard M, Tang Y, Dali R, Lo R, Stifani S, McPherson PS (2021). An Arf/Rab cascade controls the growth and invasiveness of glioblastoma. J Cell Biol 220, e202004229.

Lebeda RA, Johnson SK, Haun RS (1999). Transcriptional regulation of the human ADP-ribosylation factor 5 (ARF5) gene. Biochim Biophys Acta 1445, 314–320.

Lenoir M, Kufareva I, Abagyan R, Overduin M (2015). Membrane and protein interactions of the pleckstrin homology domain superfamily. Membranes (Basel) 5, 646–663.

Li L, Kim E, Yuan H, Inoki K, Goraksha-Hicks P, Schiesher RL, Neufeld TP, Guan KL (2010). Regulation of mTORC1 by the Rab and Arf GTPases. J Biol Chem 285, 19705–19709.

Lim CY, Zoncu R (2016). The lysosome as a command-and-control center for cellular metabolism. J Cell Biol 214, 653–664.

Lim JP, Wang JT, Kerr MC, Teasdale RD, Gleeson PA (2008). A role for SNX5 in the regulation of macropinocytosis. BMC Cell Biol 9, 58.

Lin XP, Mintern JD, Gleeson PA (2020). Macropinocytosis in different cell types: similarities and differences. Membranes (Basel) 10, 177.

Liu X, Zheng XF (2007). Endoplasmic reticulum and Golgi localization sequences for mammalian target of rapamycin. Mol Biol Cell 18, 1073–1082.

Livingstone M, Bidinosti M (2012). Rapamycin-insensitive mTORC1 activity controls eIF4E:4E-BP1 binding. F1000Res 1, 4.

Long X, Lin Y, Ortiz-Vega S, Yonezawa K, Avruch J (2005). Rheb binds and regulates the mTOR kinase. Curr Biol 15, 702–713.

Luke MR, Kjer-Nielsen L, Brown DL, Stow JL, Gleeson PA (2003). GRIP domain-mediated targeting of two new coiled-coil proteins, GCC88 and GCC185, to subcompartments of the trans-Golgi network. J Biol Chem 278, 4216–4226.

Makhoul C, Gleeson PA (2021). Regulation of mTORC1 activity by the Golgi apparatus. Fac Rev 10, 50.

Makyio H, Ohgi M, Takei T, Takahashi S, Takatsu H, Katoh Y, Hanai A, Ueda T, Kanaho Y, Xie Y, *et al*. (2012). Structural basis for Arf6-MKLP1 complex formation on the Flemming body responsible for cytokinesis. EMBO J 31, 2590–2603.

Mellstrom K, Heldin CH, Westermark B (1988). Induction of circular membrane ruffling on human fibroblasts by platelet-derived growth factor. Exp Cell Res 177, 347–359.

Moravec R, Conger KK, D'Souza R, Allison AB, Casanova JE (2012). BRAG2/GEP100/IQSec1 interacts with clathrin and regulates alpha5beta1 integrin endocytosis through activation of ADP ribosylation factor 5 (Arf5). J Biol Chem 287, 31138–31147.

Perluigi M, Di Domenico F, Butterfield DA (2015). mTOR signaling in aging and neurodegeneration: at the crossroad between metabolism dysfunction and impairment of autophagy. Neurobiol Dis 84, 39–49.

Rabanal-Ruiz Y, Byron A, Wirth A, Madsen R, Sedlackova L, Hewitt G, Nelson G, Stingele J, Wills JC, Zhang T, *et al*. (2021). mTORC1 activity is supported by spatial association with focal adhesions. J Cell Biol 220, e202004010.

Rahman H, Qasim M, Oellerich M, Asif AR (2014). Identification of the novel interacting partners of the mammalian target of rapamycin complex 1 in human CCRF-CEM and HEK293 cells. Int J Mol Sci 15, 4823–4836.

Rainero E, Howe JD, Caswell PT, Jamieson NB, Anderson K, Critchley DR, Machesky L, Norman JC (2015). Ligand-occupied integrin internalization links nutrient signaling to invasive migration. Cell Rep 10, 398–413.

Ralph P, Nakoinz I (1977). Antibody-dependent killing of erythrocyte and tumor targets by macrophage-related cell lines: enhancement by PPD and LPS. J Immunol 119, 950–954.

Rizzo MA, Springer GH, Granada B, Piston DW (2004). An improved cyan fluorescent protein variant useful for FRET. Nat Biotechnol 22, 445–449.

Sadakata T, Shinoda Y, Sekine Y, Saruta C, Itakura M, Takahashi M, Furuichi T (2010). Interaction of calcium-dependent activator protein for secretion 1 (CAPS1) with the class II ADP-ribosylation factor small GTPases is required for dense-core vesicle trafficking in the trans-Golgi network. J Biol Chem 285, 38710–38719.

Sancak Y, Bar-Peled L, Zoncu R, Markhard AL, Nada S, Sabatini DM (2010). Ragulator-Rag complex targets mTORC1 to the lysosomal surface and is necessary for its activation by amino acids. Cell 141, 290–303.

Sancak Y, Peterson TR, Shaul YD, Lindquist RA, Thoreen CC, Bar-Peled L, Sabatini DM (2008). The Rag GTPases bind raptor and mediate amino acid signaling to mTORC1. Science 320, 1496–1501.

Sarbassov DD, Ali SM, Kim DH, Guertin DA, Latek RR, Erdjument-Bromage H, Tempst P, Sabatini DM (2004). Rictor, a novel binding partner of

mTOR, defines a rapamycin-insensitive and raptor-independent pathway that regulates the cytoskeleton. Curr Biol 14, 1296–1302.
Saxton RA, Sabatini DM (2017). mTOR signaling in growth, metabolism, and disease. Cell 168, 960–976.
Sero JE, Thodeti CK, Mammoto A, Bakal C, Thomas S, Ingber DE (2011). Paxillin mediates sensing of physical cues and regulates directional cell motility by controlling lamellipodia positioning. PLoS One 6, e28303.
Sukhanova A, Gorin A, Serebriiskii IG, Gabitova L, Zheng H, Restifo D, Egleston BL, Cunningham D, Bagnyukova T, Liu H, *et al.* (2013). Targeting C4-demethylating genes in the cholesterol pathway sensitizes cancer cells to EGF receptor inhibitors via increased EGF receptor degradation. Cancer Discov 3, 96–111.
Thomas CC, Dowler S, Deak M, Alessi DR, van Aalten DM (2001). Crystal structure of the phosphatidylinositol 3,4-bisphosphate-binding pleckstrin homology (PH) domain of tandem PH-domain-containing protein 1 (TAPP1): molecular basis of lipid specificity. Biochem J 358, 287–294.
Thomas JD, Zhang YJ, Wei YH, Cho JH, Morris LE, Wang HY, Zheng XF (2014). Rab1A is an mTORC1 activator and a colorectal oncogene. Cancer Cell 26, 754–769.
Walker EH, Pacold ME, Perisic O, Stephens L, Hawkins PT, Wymann MP, Williams RL (2000). Structural determinants of phosphoinositide 3-kinase inhibition by wortmannin, LY294002, quercetin, myricetin, and staurosporine. Mol Cell 6, 909–919.
Wang L, Harris TE, Roth RA, Lawrence JC Jr (2007). PRAS40 regulates mTORC1 kinase activity by functioning as a direct inhibitor of substrate binding. J Biol Chem 282, 20036–20044.
Wang Y, Chen Z, Jia C, Bai X, Jiang Y, Zou Z (2021). Analysis of the mTOR Interactome using SILAC technology revealed NICE-4 as a novel regulator of mTORC1 activity. Life Sci 281, 119745.
Wullschleger S, Loewith R, Hall MN (2006). TOR signaling in growth and metabolism. Cell 124, 471–484.
Wymann MP, Bulgarelli-Leva G, Zvelebil MJ, Pirola L, Vanhaesebroeck B, Waterfield MD, Panayotou G (1996). Wortmannin inactivates phosphoinositide 3-kinase by covalent modification of Lys-802, a residue involved in the phosphate transfer reaction. Mol Cell Biol 16, 1722–1733.
Yadav RB, Burgos P, Parker AW, Iadevaia V, Proud CG, Allen RA, O'Connell JP, Jeshtadi A, Stubbs CD, Botchway SW (2013). mTOR direct interactions with Rheb-GTPase and raptor: sub-cellular localization using fluorescence lifetime imaging. BMC Cell Biol 14, 3.
Yang H, Jiang X, Li B, Yang HJ, Miller M, Yang A, Dhar A, Pavletich NP (2017). Mechanisms of mTORC1 activation by RHEB and inhibition by PRAS40. Nature 552, 368–373.
Yoshida S, Pacitto R, Yao Y, Inoki K, Swanson JA (2015). Growth factor signaling to mTORC1 by amino acid-laden macropinosomes. J Cell Biol 211, 159–172.
Zhang J, Kim J, Alexander A, Cai S, Tripathi DN, Dere R, Tee AR, Tait-Mulder J, Di Nardo A, Han JM, *et al.* (2013). A tuberous sclerosis complex signalling node at the peroxisome regulates mTORC1 and autophagy in response to ROS. Nat Cell Biol 15, 1186–1196.
Zhou X, Clister TL, Lowry PR, Seldin MM, Wong GW, Zhang J (2015). Dynamic visualization of mTORC1 activity in living cells. Cell Rep 10, 1767–1777.